

Attentional Biased Stochastic Gradient for Imbalanced Classification

Qi Qi

Department of Computer Science, The University of Iowa, Iowa City, IA 52242, USA

QI-QI@UIOWA.EDU

Yi Xu

Machine Intelligence Technology, Alibaba Group, Bellevue, WA 98004, USA

YIXU@ALIBABA-INC.COM

Rong Jin

Machine Intelligence Technology, Alibaba Group, Bellevue, WA 98004, USA

JINRONG.JR@ALIBABA-INC.COM

Wotao Yin

Department of Mathematics, University of California, Los Angeles, CA 90095, USA

WOTAOYIN@MATH.UCLA.EDU

Tianbao Yang

Department of Computer Science, The University of Iowa, Iowa City, IA 52242, USA

TIANBAO-YANG@UIOWA.EDU

Abstract

In this paper¹, we present a simple yet effective method (ABSGD) for addressing the data imbalance issue in deep learning. Our method is a simple modification to momentum SGD where we leverage an attentional mechanism to assign an individual importance weight to each gradient in the mini-batch. Unlike existing individual weighting methods that learn the individual weights by meta-learning on a separate balanced validation data, our weighting scheme is self-adaptive and is grounded in *distributionally robust optimization*. The weight of a sampled data is systematically proportional to exponential of a scaled loss value of the data, where the scaling factor is interpreted as the regularization parameter in the framework of information-regularized distributionally robust optimization. We employ a step damping strategy for the scaling factor to balance between the learning of feature extraction layers and the learning of the classifier layer. Compared with existing meta-learning methods that require three backward propagations for computing mini-batch stochastic gradients at three different points at each iteration, our method is more efficient with only one backward propagation at each iteration as in standard deep learning methods. Compared with existing class-level weighting schemes, our method can be applied to online learning without any knowledge of class prior, while enjoying further performance boost in offline learning combined with existing class-level weighting schemes. Our empirical studies on several benchmark datasets also demonstrate the effectiveness of our proposed method.

1. Introduction

Deep Learning (DL) has emerged as the most popular machine learning technique in recent years, especially in computer vision. It has brought transformative impact in industries and quantum leaps in the quality of a wide range of everyday technologies including face recognition (Schroff et al., 2015; Taigman et al., 2014; Parkhi et al., 2015; Wen et al., 2016; Liu et al., 2019), speech recognition (Graves et al., 2013; Chung et al., 2014; Kim, 2014; Graves, 2013; Ravanelli et al., 2018) and machine translation (Cho et al., 2014; Bahdanau et al., 2014; Sutskever et al., 2014; Luong et al., 2015; Vaswani et al., 2018). Most of these systems are built based on learning a deep neural network (DNN) model from a huge amount of data. However, it has been observed that these deep learning systems could **fail in some underrepresented cases** (Johnson and Khoshgoftaar, 2019; Lin et al., 2017; Chan et al., 2019; Fernández et al., 2018; Huang et al., 2019). For example, Apple’s FaceID (a face recognition system) is much less accurate for recognizing a child than an adult (Bud, 2018), and an autonomous driving car might fail at night under the same road condition (Wakabayashi, 2018). The key factors that cause these problems are (i) the training data sets collected from the real-world are usually **highly imbalanced** (e.g., the number of facial images of children are much less than that of adults); (ii)

1. The original title is “Momentum SGD with Robust Weighting For Imbalanced Classification”

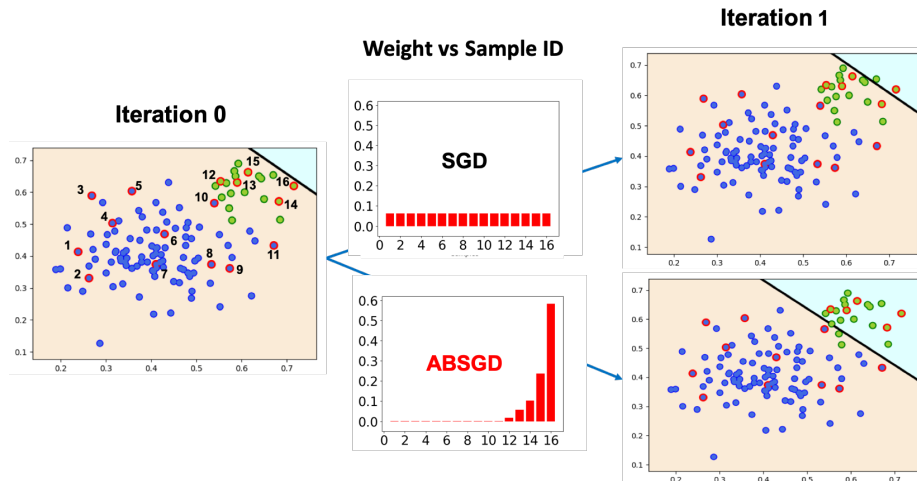


Figure 1: A two-dimensional linear binary classification toy example with logistic loss. We optimize the model for one iteration using SGD with different weighting schemes for the same stochastic minibatch. The classifier generated in iteration 1 vividly demonstrates the effectiveness of attentional biased SGD, compared to not doing it, on handling data imbalance.

current deep learning systems lack the capability to handle imbalanced data distribution well. Most modern deep learning techniques in the literature are crafted and evaluated on benchmark datasets (e.g., ImageNet data for image classification), which are created by humans intentionally with balanced distributions among different classes.

Two categories of approaches have been well studied for tackling data imbalance, i.e., under/over-sampling based approaches (Chawla et al., 2002; Han et al., 2005; Chawla, 2009) and cost-sensitive loss minimization (Zhou and Liu, 2005; Sun et al., 2007; Scott, 2011; Parambath et al., 2014; Narasimhan et al., 2015; Elkan, 2001; Busa-Fekete et al., 2015; Yan et al., 2017). These two categories of approaches have been investigated for deep learning (Johnson and Khoshgoftaar, 2019; Masko and Hensman, 2015; Lee et al., 2016; Khan et al., 2017). But existing studies in these directions are not very successful for deep learning with big data. For example, several studies have found that over-sampling yields better performance than using under-sampling (Johnson and Khoshgoftaar, 2019). But over-sampling will add more examples to the training data, which will lead to increased training time. The idea of cost-sensitive loss minimization is to assign class-level weights to data belonging to different classes aiming to balance the contributions from different classes. However, this type of methods neglect the differences between different examples in the same class despite it might require much parameter-tuning of class-level weights. Beyond the aforementioned two categories of methods, some recent works tackle the data imbalance issue from different perspectives, including crafting new individual loss functions (Cao et al., 2019), and learning individual-level weights (Jamal et al., 2020; Ren et al., 2018). For example, Jamal et al. (2020); Ren et al. (2018) proposed meta-learning methods to learn the individual weights along with updating the model parameters. These methods require maintaining a balanced validation data to update the individual weights for sampled data and require multiple backward propagations at each iteration, which incurs additional significant burden for training an neural network on big data.

In this paper, we propose a simple yet systematic **attentional biased stochastic gradient descent** (ABSGD) method for addressing the data imbalance issue. Our method is a simple modification of the popular momentum SGD method for deep learning by injecting individual-level importance weights to stochastic gradients in the mini-batch. These importance weights allow our method to focus on hard examples using an attentional mechanism. Unlike existing attention models that learn attentional weights on more fine-grained level (e.g., words in language (Vaswani et al., 2017), and regions in images (Posner et al., 1980)), our method is using the attention on the level of samples in a mini-batch. This idea is illustrated in Figure 1 on a toy

imbalanced dataset by comparing it with the standard momentum SGD method for deep learning. Unlike existing meta-learning methods, our individual-level weights are self-adaptive that are computed based on the loss value of each individual data. In particular, the weight for each example is proportional to exponential of a scaled loss value on that example. The weighting scheme is **grounded in the theoretically justified distributionally robust optimization (DRO) framework** for learning with imbalanced data. Specifically, our method can be considered as a stochastic momentum method for solving an information-regularized distributionally robust optimization (IR-DRO) problem (Zhu et al., 2019) defined on all possible data. From this perspective, our method has several unique features. (i) The weights for all examples in the mini-batch have a proper normalization term to ensure the method optimizes the IR-DRO problem, which is updated online. We prove a theorem to show that our method converges to a stationary solution of the non-convex IR-DRO problem (with a certain convergence rate). (ii) The scaling factor before the loss value in the exponential function is interpreted as the regularization parameter in the DRO framework. In order to balance between the learning of feature extraction layers and the learning of the classifier layer of a DNN, we employ a step damping strategy for the scaling factor in our method. In addition, our method has two benefits: (i) it is applicable in online learning, where the data is received sequentially; (ii) it is loss independent, and can be combined with all existing loss functions crafted for tackling data imbalance. Finally, we summarize **our contributions** below:

- We propose a simple attentional biased stochastic gradient descent method with momentum and self-adaptive importance weighting to tackle deep learning with imbalanced data, which is named as **ABSGD**.
- We prove that ABSGD finds a stationary solution of a non-convex information-regularized distributionally robust optimization problem for learning a deep neural network, and establish its convergence rate.
- We compare ABSGD with a variety of existing methods for addressing the data imbalance issue, including crafted loss functions, class-balancing weighting methods, meta-learning methods for individual-level weighting, and demonstrate superb performance of ABSGD.

2. Related Work

In this section, we provide a review on related work for addressing the issue of data imbalance. We will focus on four categories of methods.

Class-level Weighting. The idea of class-level weighting is to introduce weights to examples at the class level to balance the contributions from different classes. This idea is rooted in cost-sensitive classification in machine learning (Ling and Sheng, 2008). Typically, the class-wise weights are proportional to the inverse of class sizes (Huang et al., 2016; Yin et al., 2018). Cui et al. (2019) proposed an improved class-level weighting scheme according to inverse of the “effective number” of examples per class. It is also notable that over/under-sampling methods have the same effect of introducing the class-level weighting to the training algorithm. We can see that these class-level weighting schemes usually require certain knowledge about the size (distribution) of each class, which makes them not suitable to online learning where the size of each class is not known beforehand. These methods also neglect the differences between different examples from the same class (cf. Figure 1).

Crafted Individual Loss Functions. Some crafted individual loss functions have been proposed for tackling data imbalance. A popular loss function is known as the focal loss (Lin et al., 2017), which is a modification of the standard cross-entropy loss. Specifically, it is defined as $-(1 - p_t)^\gamma \log(p_t)$ where $\gamma > 0$ is a tuning parameter p_t is the estimated probability for the ground-truth class. The focal loss has been observed to be effective for dense object detection and is also widely used for classification with imbalanced data due to its simplicity (Goyal and Kaiming, 2018). However, the focal loss lacks theoretical foundation. To complement this, Cao et al. (2019) proposed a theoretically-principled label-distribution-aware margin loss, which injects uneven margins into the cross-entropy loss, where the margin for each class is proportional to inverse of each

class size to the power of 1/4. Our method is loss independent and hence can be combined with these existing crafted individual loss functions.

Meta-Learning Methods. Meta-learning methods have been proposed for improving the performance on imbalanced datasets. The idea is to learn individual-level weights by solving a two-level optimization problem. In particular,

$$\min_{\theta} \frac{1}{|\mathcal{C}|} \sum_{\mathbf{z}_i \in \mathcal{C}} L(\mathbf{w}(\theta); \mathbf{z}_i), \quad \text{where}$$

$$\mathbf{w}(\theta) = \arg \min_{\mathbf{w}} \frac{1}{|\mathcal{D}|} \sum_{\mathbf{z}_i \in \mathcal{D}} \theta_i L(\mathbf{w}; \mathbf{z}_i),$$

where \mathcal{D} denotes the training dataset, \mathcal{C} denotes a balanced validation dataset, \mathbf{w} denotes the model parameter, \mathbf{z}_i denotes a data, $L(\mathbf{w}; \mathbf{z})$ denotes the loss value of model \mathbf{w} on data \mathbf{z} , and $\theta = (\theta_1, \dots, \theta_{|\mathcal{D}|})$ denotes the weights on the training examples. Ren et al. (2018) directly optimized the individual weights in the framework of meta-learning with a heuristic trick by normalizing the weights of all examples in a training batch so that they sum up to one. Jamal et al. (2020) considered the problem from the perspective of domain adaptation and decomposed the individual weight into sum of a non-learnable class-level weight and a learnable individual-level weight. One issue of these meta-learning methods is that they require three back-propagations at each iteration, which is computationally more expensive than our method that is about the same cost of standard SGD for DL.

Optimization of DRO. DRO is a useful technique for domain adaptation, which has been shown both theoretically and empirically promising for learning with imbalanced data (Shalev-Shwartz and Wexler, 2016; Namkoong and Duchi, 2017; Qi et al., 2019). However, most existing optimization algorithms for DRO are not practical for deep learning, which dims the usefulness of DRO. In the literature, DRO is formulated as (Rahimian and Mehrotra, 2019; Namkoong and Duchi, 2017) :

$$\min_{\mathbf{w} \in \mathbb{R}^d} \max_{\mathbf{p} \in \Delta_n} \sum_{i=1}^n p_i L(\mathbf{w}; \mathbf{z}_i) - h(\mathbf{p}, \mathbf{1}/n) + r(\mathbf{w}), \quad (1)$$

where $\Delta_n = \{\mathbf{p} \in \mathbb{R}^n : \sum_i p_i = 1, p_i \geq 0\}$ denotes an n -dimensional simplex, $h(\mathbf{p}, \mathbf{1}/n)$ is a divergence measure or constraint between \mathbf{p} and uniform probabilities $\mathbf{1}/n$, $r(\mathbf{w})$ is a standard regularizer on \mathbf{w} . We can see DRO aims to minimize the worst-case loss over all the underlying distribution \mathbf{p} in an uncertainty set specified by $h(\mathbf{p}, \mathbf{1}/n)$. Many primal-dual optimization algorithms have been designed for solving the above problem for DL (Rafique et al., 2018; Yan et al., 2020). However, the dual variable \mathbf{p} in the above min-max form is an n -dimensional variable restricted to a simplex, which makes existing primal-dual optimization algorithms computationally expensive and not applicable for the online setting where the data is coming sequentially. Our method can be considered as a solution to addressing these issues by considering a specific information-oriented regularizer $h(\mathbf{p}, \mathbf{1}/n) = \lambda \sum_i p_i \log(np_i)$ that is the KL divergence between \mathbf{p} and uniform probabilities $\mathbf{1}/n$, which allows us to transform the min-max formulation into an equivalent minimization formulation with a compositional objective. From this perspective, our method resembles a recently proposed dual-free algorithm RECOVER (Qi et al., 2020). However, RECOVER requires computing stochastic gradients at two different points in each iteration, which causes their GPU cost to double ours. In addition, RECOVER is a variance-reduction method, which might have poor generalization performance.

3. Attentional Biased SGD with Momentum (ABSGD)

In this section, we present the proposed method ABSGD and its analysis. We first describe the algorithm and then connect it to the DRO framework. Then we present the convergence result of our method for solving IR-DRO. Throughout this paper, we let $\mathbf{z} = (\mathbf{x}, y)$ denote a random sample that includes an input $\mathbf{x} \in \mathbb{R}^d$ and a ground truth label $y \in \{1, \dots, K\}$, $\mathbf{w} \in \mathbb{R}^d$ denote the weight of the underlying DNN to be learned. Let $\mathbf{f}(\mathbf{x}) \in \mathbb{R}^K$ be the prediction score of the DNN on data \mathbf{x} , and $\ell(\mathbf{f}; y)$ denote a loss function. For simplicity, we let $L(\mathbf{w}; \mathbf{z}) = \ell(\mathbf{f}(\mathbf{x}); y)$. A standard loss function is the cross-entropy loss where

$\ell(\mathbf{f}; y) = -\log \frac{\exp(f_y(\mathbf{x}))}{\sum_{k=1}^K \exp(f_k(\mathbf{x}))}$. We emphasize that our method is loss independent, and can be applied with any loss functions $\ell(\mathbf{f}; y)$. More importantly, we can employ the class-level weighted loss functions such as the class-balanced loss (Cui et al., 2019), crafted individual loss functions such as label-distribution aware margin loss (Cao et al., 2019)

3.1 Algorithm

The proposed algorithm ABSGD is presented in Algorithm 1. The key steps are described in Step 4 to Step 8, and the key updating step for \mathbf{w}_{t+1} is given by

$$\mathbf{w}_{t+1} = \mathbf{w}_t - \eta \left(\frac{1}{B} \sum_{i=1}^B \tilde{p}_i \nabla L(\mathbf{w}_t; \mathbf{z}_i) + \nabla r(\mathbf{w}_t) \right) + \beta(\mathbf{w}_t - \mathbf{w}_{t-1}) \quad (2)$$

where $r(\mathbf{w}) \propto 1/2 \|\mathbf{w}\|_2^2$ denotes a standard ℓ_2 norm regularization (i.e., for contributing weight decay in the update). The above update is a simple modification of the standard momentum method (Polyak, 1964), where the last term $\beta(\mathbf{w}_t - \mathbf{w}_{t-1})$ is a momentum term. The modification lies at the introduced weight \tilde{p}_i for each data \mathbf{z}_i in the mini-batch. The individual weight \tilde{p}_i is computed in Step 7 and is proportional to $\exp(L(\mathbf{w}_t; \mathbf{z}_i)/\lambda)$, where λ is a scaling parameter. Intuitively, we can see that a sample with a large loss value tends to get a higher weight. It makes sense for learning with imbalanced data since the model leans towards fitting the data from the majority class well rendering the loss value on the minority class larger. Hence, the data from the minority class tends to get a larger weight \tilde{p}_i . This phenomenon is demonstrated on a toy dataset in Figure 1.

There are several other features of Algorithm 1 that deserves further discussion. First, the weight \tilde{p}_i is properly normalized dividing a quantity s_{t+1} that is updated online. In particular, s_{t+1} maintains a moving average of exponential of the scaled loss value on the sampled data (Step 6). It is notable that the normalization does not make the sum of \tilde{p}_i in the mini-batch equal to 1. We emphasize that this normalization is essential in twofold: (i) it stabilizes the update without causing any numerical issue; (ii) it ensures the algorithm converge to a meaningful solution as presented in next subsection. Second, the algorithm has two stages divided by the value changing of λ . This has a connection to the regularization impact of λ . With larger λ , our method is getting close to the standard momentum SGD method without weighting. In particular, when $\lambda = \infty$, the update becomes the standard momentum SGD method. When λ becomes smaller, the update will focus more on data with larger loss values (e.g., from the minority class). This uneven weighting is helpful to learn a robust classifier. However, it harms the learning of feature extraction layers. This phenomenon has been also observed in previous works (Cao et al., 2019). Hence, to address this issue we design a step damping strategy for λ by dividing the learning into two. For example, in the first stage, we use a larger value of λ_0 to facilitate the learning of feature extraction layers and in the second stage we decrease the value of λ to a smaller value $\lambda_1 < \lambda_0$ to facilitate the learning of classifier. It is notable that in the second stage, we also need to reset $s_{T_0} = 0$ due to the value change of λ . Also note that this two-stage scheme can be extended to multiple stages with a decreasing sequence of λ . Finally, in Algorithm 1 we allow the learning rate η to be annealed after some iterations following the standard learning rate strategy for the momentum SGD method (Krizhevsky et al., 2017).

3.2 Connection with DRO

In this subsection, we explain ABSGD by connecting it to the framework of DRO. In particular, given n training samples $\{\mathbf{z}_1, \dots, \mathbf{z}_n\}$ we consider the following information-regularized DRO formulation

$$\min_{\mathbf{w} \in \mathbb{R}^d} \max_{\mathbf{p} \in \Delta_n} F(\mathbf{w}, \mathbf{p}) = \sum_{i=1}^n p_i L(\mathbf{w}; \mathbf{z}_i) - \lambda \sum_i p_i \ln(np_i) + r(\mathbf{w}). \quad (3)$$

Algorithm 1 ABSGD

- 1: **Require:** $\lambda_0 > \lambda_1, T_0, T_1, \gamma \in (0, 1), \beta \in (0, 1), \eta$
 - 2: **Initialize** \mathbf{w}_1 randomly,
 - 3: Set $\lambda = \lambda_0$, and $s_0 = 0$ ◊ Stage I
 - 4: **for** $t = 1, \dots, T_0$ **do**
 - 5: Sample/Receive a mini-batch of B samples $\{\mathbf{z}_1, \dots, \mathbf{z}_B\}$
 - 6: Compute $\tilde{g}(\mathbf{w}_t) = \frac{1}{B} \sum_{i=1}^B \exp(L(\mathbf{w}_t, \mathbf{z}_i)/\lambda)$
 - 7: Compute $s_{t+1} = (1 - \gamma)s_t + \gamma\tilde{g}(\mathbf{w}_t)$
 - 8: Compute $\tilde{p}_i = \frac{\exp(\frac{L(\mathbf{w}_t, \mathbf{z}_i)}{\lambda})}{s_{t+1}}$, for $i = 1, \dots, B$
 - 9: Update \mathbf{w}_{t+1} by Equation (2)
 - 10: **end for**
 - 11: Set $\lambda = \lambda_1, s_{T_0} = 0$ ◊Reset λ, s for Stage II
 - 12: Optional: $\eta = \eta/\tau$: anneal η by a factor τ if necessary
 - 13: **for** $t = T_0 + 1, \dots, T_0 + T_1$ **do**
 - 14: Repeat Steps 4 ~ 10 as in the Stage I
 - 15: Optional: anneal η after some iterations if necessary
 - 16: **end for**
 - 17: Optional: Add more stages with smaller λ if necessary
-

Note that unlike many existing studies of DRO that regularizes \mathbf{p} by a constraint, we use the KL divergence between \mathbf{p} and $1/n$ as regularization function, i.e., use $\lambda \sum_i^n p_i \ln(np_i)$ to regularize \mathbf{p} , where λ is the regularizer parameter.

Robustness of DRO. The DRO framework can be understood as a way of addressing domain adaptation. In particular, the empirical uniform distribution over training examples $\{\mathbf{z}_1, \dots, \mathbf{z}_n\}$ does not necessarily represent the distribution in testing data. Hence by introducing the non-uniform probabilities \mathbf{p} we can capture the domain shift between training data and the testing data. There is an interesting observation regarding λ . When $\lambda = \infty$, then $p_i = 1/n$ and the above problem becomes the standard empirical risk minimization problem:

$$\min_{\mathbf{w} \in \mathbb{R}^d} \frac{1}{n} \sum_{i=1}^n L(\mathbf{w}; \mathbf{z}_i) + r(\mathbf{w}).$$

When $\lambda = 0$, then \mathbf{p} has only one component equal to 1 that corresponds to the data with largest loss value, and the problem becomes the maximal loss minimization:

$$\min_{\mathbf{w} \in \mathbb{R}^d} \max_i L(\mathbf{w}; \mathbf{z}_i) + r(\mathbf{w}).$$

The above maximal loss minimization has been studied for learning with imbalanced data (Shalev-Shwartz and Wexler, 2016). It was shown theoretically to yield better generalization performance than empirical risk minimization. However, the maximal loss minimization is sensitive to outliers. Hence, by varying the value of λ we can enjoy balanced robustness to the imbalanced data and outliers.

Optimization of DRO. It is nice that the DRO formulation is robust to imbalanced data. However, the min-max formulation of DRO is not friendly to the design of efficient optimization algorithms, especially given the constraint $\mathbf{p} \in \Delta_n$. To this end, we follow Qi et al. (2020) to transform the min-max formulation into an equivalent minimization formulation. In particular, we first compute the optimal solution of dual variable \mathbf{p}^* for the inner maximization problem given \mathbf{w} . By computing the first-derivation of equation (3) in terms of \mathbf{p}

and setting it to zero, *i.e.* $\nabla_{\mathbf{p}} F(\mathbf{w}, \mathbf{p}) = 0$, we have \mathbf{p}^* :

$$p_i^* = \frac{\exp(\frac{L(\mathbf{w}; \mathbf{z}_i)}{\lambda})}{\sum_{i=1}^n \exp(\frac{L(\mathbf{w}; \mathbf{z}_i)}{\lambda})}, \quad i = 1, \dots, n \quad (4)$$

By substituting \mathbf{p}^* into the min-max problem of DRO, we obtain the following equivalent minimization formulation:

$$\min_{\mathbf{w} \in \mathbb{R}^d} F_\lambda(\mathbf{w}) = \lambda \ln \left(\frac{1}{n} \sum_{i=1}^n \exp(L(\mathbf{w}; \mathbf{z}_i)/\lambda) \right) + r(\mathbf{w}). \quad (5)$$

In an online learning setting, we can further generalize the above formulation as

$$\min_{\mathbf{w} \in \mathbb{R}^d} F_\lambda(\mathbf{w}) = \lambda \ln (\mathbb{E}_{\mathbf{z}} \exp(L(\mathbf{w}; \mathbf{z})/\lambda)) + r(\mathbf{w}). \quad (6)$$

Given the above minimization formulations, our method ABSGD can be considered as a stochastic algorithm for optimizing (5) in offline learning or optimizing (6) in online learning. Our method is rooted in stochastic optimization for compositional optimization that has been studied in the literature (Wang et al., 2017; Chen et al., 2020; Qi et al., 2020). Intuitively, we can understand our weighting scheme $\tilde{\mathbf{p}}$ as following. In offline learning with a big data size where n is huge, it is impossible to calculate the \mathbf{p}^* as in (4) at every iteration due to computation and memory limits. As a result, we need to approximate \mathbf{p}^* in a systematic way. In our method, we use moving average estimate s_{t+1} to approximate the denominator in \mathbf{p}^* , *i.e.*, $\frac{1}{n} \sum_{i=1}^n \exp(\frac{L(\mathbf{w}; \mathbf{z}_i)}{\lambda})$, and use it to compute a scaled weight of data in the mini-batch by Step 7, *i.e.*,

$$\tilde{p}_i = \frac{\exp(\frac{L(\mathbf{w}_t; \mathbf{z}_i)}{\lambda})}{s_{t+1}}, \quad i \in \{1, \dots, B\}. \quad (7)$$

More rigorously, our method ABSGD is a stochastic momentum method for solving a compositional problem in the form $f(g(\mathbf{w})) + r(\mathbf{w})$. To this end, we write the objective in (6) as $f(g(\mathbf{w})) + r(\mathbf{w})$, where $f(g) = \lambda \log(g)$ and $g(\mathbf{w}) = \mathbb{E}_{\mathbf{z}}[\exp(L(\mathbf{w}; \mathbf{z})/\lambda)]$. The difficulty of stochastic optimization for the compositional function $f(g(\mathbf{w}))$ lies on computing an approximate gradient at \mathbf{w}_t . By the chain rule, its gradient is given by $\nabla f(g(\mathbf{w}_t))^T \nabla g(\mathbf{w}_t)$, where $\nabla g(\mathbf{w}_t)$ can be estimated by mini-batch stochastic gradient, *i.e.*, $\frac{1}{B} \sum_{i=1}^B \exp(L(\mathbf{w}_t; \mathbf{z}_i)/\lambda) \frac{\nabla L(\mathbf{w}_t; \mathbf{z}_i)}{\lambda}$. To approximate $\nabla f(g(\mathbf{w}_t)) = \frac{\lambda}{g(\mathbf{w}_t)}$, we use a moving average to estimate $g(\mathbf{w}_t)$ inspired by (Wang et al., 2017), which is updated in Step 6, *i.e.*,

$$s_{t+1} = (1 - \gamma)s_t + \gamma \tilde{g}(\mathbf{w}_t), \quad \text{where}$$

$$\tilde{g}(\mathbf{w}_t) = \frac{1}{B} \sum_{i=1}^B \exp\left(\frac{L(\mathbf{w}_t; \mathbf{z}_i)}{\lambda}\right).$$

Hence, the true gradient $\nabla f(g(\mathbf{w}_t))^T \nabla g(\mathbf{w}_t)$ is able to be approximated by

$$\frac{\lambda}{s_{t+1}} \nabla \tilde{g}(\mathbf{w}_t) = \frac{1}{B} \sum_{i=1}^B \frac{1}{s_{t+1}} \exp(L(\mathbf{w}_t; \mathbf{z}_i)/\lambda) \nabla L(\mathbf{w}_t; \mathbf{z}_i),$$

which is exactly the approximate gradient used in the update of \mathbf{w}_{t+1} as in equation (2). Note that, different from (Wang et al., 2017; Chen et al., 2020; Qi et al., 2020) on stochastic optimization for a compositional function, we employ the momentum term to improve the convergence and generalization performance.

3.3 Convergence Analysis

In this subsection, we provide a convergence result of ABSGD for solving the DRO objective under some standard assumptions in non-convex optimization. In particular, we focus on the online formulation in (6). For presentation simplicity, we use the notations $g(\mathbf{w}) = \mathbb{E}_{\mathbf{z}}[\exp(L(\mathbf{w}; \mathbf{z})/\lambda)]$ and $g(\mathbf{w}; \mathbf{z}) = \exp(L(\mathbf{w}; \mathbf{z})/\lambda)$. We first state a standard assumption (Qi et al., 2020; Wang et al., 2017) and then present our main theorem.

Assumption 1 For a fixed $\lambda = \lambda_1$, there exists $V_g > 0$ such that

$$\mathbb{E}_{\mathbf{z}}[\|g(\mathbf{w}; \mathbf{z}) - g(\mathbf{w})\|^2] \leq V_g, \text{ and} \quad (8)$$

$$\mathbb{E}_{\mathbf{z}}[\|\nabla g(\mathbf{w}; \mathbf{z}) - \nabla g(\mathbf{w})\|^2] \leq V_g \quad (9)$$

and $L(\mathbf{w}; \mathbf{z})$ for any \mathbf{z} is an L -smooth function, i.e.,

$$\|\nabla L(\mathbf{w}; \mathbf{z}) - \nabla L(\mathbf{w}'; \mathbf{z})\| \leq L\|\mathbf{w} - \mathbf{w}'\|, \forall \mathbf{w}, \mathbf{w}'. \quad (10)$$

Theorem 1 Let assume assumption 1 holds. Also assume there exists C, G, Δ_0 such that $\exp(L(\mathbf{w}_t; \mathbf{z}_i)/\lambda_1) < C$, $\mathbb{E}[\|\nabla L(\mathbf{w}_t; \mathbf{z}_i)\|^2] \leq G$, for all $\mathbf{w}_t, \mathbf{z}_i$, and $F_{\lambda_1}(\mathbf{w}_{T_0}) - \min_{\mathbf{w}} F_{\lambda_1}(\mathbf{w}) \leq \Delta_0$. In Algorithm 1, let $\eta = T_1^{-3/4}$ and $\gamma = T_1^{-1/2}$. Then, after T_1 iterations of ABSGD in Stage II we have

$$\frac{1}{T_1} \sum_{t=1}^{T_1} \mathbb{E}[\|\nabla F_{\lambda_1}(\mathbf{w}_{T_0+t})\|^2] \leq O\left(\frac{1}{T_1^{1/4}}\right) \quad (11)$$

where we exhibit the constant in the big O in appendix.

Remark: The above theorem implies that a randomly chosen solution in Stage II will converge to the stationary point of the objective $F_{\lambda_1}(\mathbf{w})$ when $T_1 \rightarrow \infty$. The convergence rate in the order of $1/T_1^{1/4}$ is the same as the stochastic method for solving compositional optimization problem (Wang et al., 2017). It is notable that we can also use an advanced technique to update s_{t+1} according to (Chen et al., 2020)

$$s_{t+1} = (1 - \gamma)(s_t + \nabla \tilde{g}(\mathbf{w}_t)^T(\mathbf{w}_t - \mathbf{w}_{t-1})) + \gamma \tilde{g}(\mathbf{w}_t)$$

and we are able to prove a convergence rate in the order of $1/T_1^{1/2}$ similar to the convergence rate of standard SGD for empirical risk minimization. In practice, we observe that the two methods have similar performance and since the convergence analysis is not the focus of this paper, we defer the improved convergence rate analysis to the appendix for the interested readers.

4. Experiments

We conduct experiments on imbalanced benchmark datasets, including CIFAR-10 (LT), CIFAR-10 (ST), CIFAR-100 (LT), CIFAR-100 (ST), Imagenet-LT (Liu et al., 2019), Places-LT (Zhou et al., 2017), which are manually created for evaluating different methods for tackling data imbalance. We provide details of these datasets shortly. We also compare with state-of-the-art methods on inherently imbalanced dataset iNaturalist2018 (iNaturalist, 2018). Finally, we provide some ablation studies on the proposed method.

For our method ABSGD, we tune λ_1 in $\{100, 200\}$, and tune λ_2 in $\{0.1, 1, 5, 10\}$. The momentum parameter is set to 0.9 in all of our experiments. We use a weight decay parameter $2e-4$ for CIFAR10, CIFAR100, $5e-4$ for Imagenet-LT and Places-LT, $1e-4$ for iNaturalist2018. ResNets (He et al., 2016) networks are the main backbone in our experiments. For baseline methods that are implemented by us, we use the momentum SGD method with the same momentum parameter, weight decay and step size. For baselines that are not implemented by us, we directly cite the results from the original paper.

Table 1: Top-1 testing accuracy (%) of ResNet32 on imbalanced CIFAR-10 and CIFAR-100 trained with label-distribution independent losses, which is suitable in online learning.

Dataset	Imbalance Type	long-tailed (LT)		step (ST)	
	Imbalance Ratio	100	10	100	10
Cifar10	SGD (CE) (Cui et al., 2019)	70.36	86.39	63.30	82.50
	ABSGD (CE)	73.10	87.94	70.89	85.78
	SGD (Focal)(Cui et al., 2019)	70.38	86.96	63.91	83.64
	ABSGD (Focal)	72.39	87.01	67.59	84.91
Cifar100	SGD (CE) (Cui et al., 2019)	34.84	55.70	38.55	54.63
	ABSGD (CE)	40.30	57.40	39.46	55.18
	SGD (Focal)(Cui et al., 2019)	38.41	55.78	38.57	53.46
	ABSGD (Focal)	39.75	57.42	39.43	55.49

4.1 Experimental Results on CIFAR Datasets

The original CIFAR-10 and CIFAR-100 data contain 50,000 training images and 10,000 validation with 10 and 100 classes, respectively. We construct the imbalanced version of training set of CIFAR10, CIFAR100 following the two strategies: Long-Tailed (LT) imbalance (Cao et al., 2019) and Step (ST) imbalance (Buda et al., 2018) with two different imbalance ratio $\rho = 10, \rho = 100$, and keep the testing set unchanged. The imbalance ratio ρ is defined as the ratio between sample sizes of the most frequent and least frequent classes. The LT imbalance follows the exponentially decayed sample size between different categories. In ST imbalance, the number of examples is equal within minority classes and equal within majority classes but differs between the majority and minority classes. We denote the imbalanced versions of CIFAR10, CIFAR100 as CIFAR10-LT/ST, CIFAR100-LT/ST according the imbalanced strategies. We adopt a stagewise training strategy with initial learning rate 0.1 and decays by a factor 10 to 160-th, 180-th epoch, respectively. We decay the value of λ at 160 epoch. The batch size is 100.

Results of using Label-Distribution Independent Losses. We first compare the effectiveness of our method compared with standard DL methods. In particular, we consider two loss functions, cross-entropy (CE) loss and focal loss. The baseline method is the momentum SGD optimizing these losses, denoted by SGD (CE) and SGD (Focal). Our methods are denoted by ABSGD (CE) and ABSGD (Focal) that employ the two losses in our framework. This comparison is meaningful as in the online learning setting the prior knowledge of class-frequency is not known. The results are reported in Table 1. We can see that ABSGD consistently outperforms SGD with a noticeable margin regardless of imbalance strategies and imbalance ration ρ . In particular, we have improvements of more than 2%, 3% on the CIFAR10-LT, and CIFAR10-ST, respectively.

Results of using Label-distribution Dependent Losses. Next, we compare ABSGD with baseline methods that use label-distribution dependent losses. In particular, we consider class-balanced versions of three individual losses, including CE loss, focal loss, label-distribution-aware margin (LDAM) loss (Cao et al., 2019). The class-balanced weighing strategy is from (Cui et al., 2019), which uses the effective number of samples to define the weight. As a result, there are three categories of class-balanced (CB) losses, i.e., CB-CE, CB-Focal, CB-LDAM. For each of these losses, we consider two optimization methods. The first method is the standard momentum SGD method with a practical trick that defers adding the class-level weighting after a number of pre-training steps with no class-level weights. This trick has been found useful to improve the performance of imbalanced data (Cao et al., 2019). We denote the first method by SGD (XX), where XX denotes the loss function. The second method is the meta learning method (Jamal et al., 2020) that uses meta-learning on a separate validation data to learn individual weights and combines them with class-balanced weights. The meta learning method has been observed with state-of-the-art results on these benchmark imbalanced datasets. We let META (XX) denote the second method. Our method is denoted by ABSGD (XX).

The results are reported in Table 2. We have the following observations regarding the results. (i) Comparing ABSGD with SGD, we can see that our method that incorporates the self-adaptive robust weighting scheme performs consistently better in almost all imbalanced settings. This verifies that the proposed self-

Table 2: Top-1 testing accuracy (%) of ResNet32 on imbalanced CIFAR-10 and CIFAR-100 trained with label-distribution dependent losses. The **red** numbers indicate the best in each category of class-weighted loss. The **bold red** numbers indicate the best in each imbalanced setting. The original paper of META does not include the results on the ST imbalanced setting, hence their missing results are marked by $-$.

Datasets	Imbalanced CIFAR-10				Imbalanced CIFAR-100			
	long-tailed		step		long-tailed		step	
Imbalance Ratio	100	10	100	10	100	10	100	10
Resampling (CE)	71.78	86.99	61.16	84.59	38.87	56.92	38.84	54.35
SGD (CB-CE) (Cui et al., 2019)	72.37	86.77	61.84	83.80	38.70	57.56	21.31	53.39
META (CB-CE) (Jamal et al., 2020)	76.41	88.85	-	-	43.35	59.58	-	-
ABSGD (CB-CE)	79.48	88.57	70.87	88.42	45.43	59.71	38.47	58.20
SGD (CB-Focal)(Cui et al., 2019)	74.57	87.10	60.27	83.46	36.02	57.99	19.76	50.02
META (CB-Focal) (Jamal et al., 2020)	78.90	88.37	-	-	44.70	59.59	-	-
ABSGD (CB-Focal)	79.14	87.04	74.85	85.90	42.48	56.69	39.24	55.36
SGD (LDAM) (Cao et al., 2019)	73.35	86.69	66.58	85.00	39.60	56.91	39.58	56.27
SGD (CB-LDAM) (Cao et al., 2019)	77.03	88.12	76.92	87.81	42.04	58.71	45.36	59.46
META (CB-LDAM) (Jamal et al., 2020)	80.00	87.40	-	-	44.08	58.80	-	-
ABSGD (CB-LDAM)	79.84	88.27	78.33	88.40	44.87	59.56	46.40	58.72

Table 3: Top-1 testing accuracy (%) on ImageNet-LT and Places-LT results.

Dataset	ImageNet-LT		Places-LT	
	Top-1	Top-5	Top-1	Top-5
CE (Jamal et al., 2020)	25.26	47.88	27.00	58.56
CB-CE (Jamal et al., 2020)	26.59	49.51	28.86	58.04
META (Jamal et al., 2020)	29.90	54.82	30.80	62.00
ABSGD (CB-CE)	32.63	57.38	33.00	64.19

adaptive weighting scheme is effective. (ii) Comparing ABSGD with META, we can see that our method performs better on CIFAR100-LT and performs slightly worse on CIFAR10-LT. It is notable that META requires a separate validation data and is more computationally expensive than our method. Hence, our method is a strong choice even compared with the state-of-the-art meta learning method.

4.2 Experimental Results on ImageNet-LT and Places-LT

ImageNet-LT (Liu et al., 2019) is a long-tailed subset of the original ImageNet-2012 by sampling a subset following the Pareto distribution with the power value 6. It has 115.8K images from 1000 categories, which include 4980 for the head class and 5 images for the tail class. The Places-LT dataset was also created by sampling from Places-2 (Zhou et al., 2017) using the same strategy as ImageNet-LT. It contains 62.5K training images from 365 classes with an imbalance ration $\rho = 4980/5$. We compare our method with the meta learning method (META) (Jamal et al., 2020), and also include two other baseline methods reported in (Jamal et al., 2020). Similar to (Jamal et al., 2020), we train ResNet32 on ImageNet-LT from scratch and train ResNet152 on Places-LT from a pretrained net trained on ImageNet data. The initial learning rate is 0.2 for ImageNet-LT and 0.01 for Places-LT, using the cosine annealing schedule (Loshchilov and Hutter, 2016) with 90 and 30 epochs, respectively. λ is decayed at 60th epoch for ImageNet-LT and 20th epoch for Places-LT.

The experimental results are reported in Table 3. From Table 3 we can see that, our ABSGD outperforms the META method and other baselines in both ImageNet-LT and Places-LT by more than 2%, which implies that our self-adaptive weighting strategy is effective. It is notable that the results in Table 3 are not comparable to the state-of-the-art results reported on these datasets. In Appendix, we combine our method with a useful trick for learning with imbalanced data (Kang et al., 2019), i.e., split the training into two stages and learn different parameters in different stages, and observe competitive results as the state-of-the-art results.

Table 4: Top-1 testing accuracy(%) of different methods on iNaturalist2018 using ResNet50, ResNet152 with ImageNet pretrained initialization and training for 90, 200 epochs in the first stage, respectively. TV represents Trainable Variable, CB denotes Class-Balanced Weighting or Sampling (Cui et al., 2019), FC represents fully connected layer, LB represents the last block in the backbone. † represents an additional balanced data set is required in the second stage. All represents standard training process that optimizing all the parameters of the backbone.

Methods Network	Stage-2 TV	Results (90)	Results (200)
		ResNet50	ResNet152
LDAM (Cao et al., 2019)	-	68.0	-
CB-CE (Cui et al., 2019)	-	65.3	-
CB-Focal (Cui et al., 2019)	-	61.1	-
NCM (CE) (Kang et al., 2019)	FC	65.2	67.3
cRT (CB-CE) (Kang et al., 2019)	FC	65.2	71.2
τ -Normalized (CE) (Kang et al., 2019)	FC	65.6	72.5
LWS (CB-CE) (Kang et al., 2019)	FC	65.9	72.1
META† (CB-CE) (Jamal et al., 2020)	All	67.6	-
META† (CB-Focal) (Jamal et al., 2020)	All	67.7	-
ABSGD (CB-CE)	FC+LB	68.5	73.1

4.3 Experimental Results on iNaturalist 2018

iNaturalist 2018 is a real world dataset whose class-frequency follows a heavy-tail distribution (iNaturalist, 2018). It contains 437K images from 8142 classes. All methods train ResNet50, ResNet152 from the corresponding pretrained models on the ImageNet. In this section, we compare ABSGD with STOA methods, which includes single-stage, two-stage and meta-learning method.

For baselines, we include momentum SGD for optimizing LDAM loss, CB-CE loss and CB-Focal loss. They are all single-stage methods. NCM (CE) and cRT (CB-CE), τ -normalized (CB-CE), LWS (CB-CE) are two-stage methods (Kang et al., 2019), where the first stage uses the standard uniform sampling to train the model with the CE loss, and the second stage fine tunes some parameters as indicated in the second column of Table 4. META is the meta-learning method (Jamal et al., 2020), which also combines the two-stage strategy for improving the performance.

Similar to the two-stage methods (Kang et al., 2019), we can optimize different set of network parameters in our method to boost the performance. We set λ to a large value $\lambda_1 \rightarrow \infty$ in the first stage. Then we decrease it to $\lambda_2 \in \{100, 200\}$, and to $\lambda_3 \in \{10, 20, 30\}$ in the second and third stages, in which we only fine-tune the FC classifiers and the last block of the neural network. For fair comparison, we follow the setting in (Kang et al., 2019; Jamal et al., 2020) that we optimize ResNet50 backbone by ABSGD with 90, 20, 10 epochs and ResNet152 backbone by ABSGD with 200, 20, 10 epochs in the three stages respectively. The batch size is 512. We also adopt the cosine annealing schedule (Loshchilov and Hutter, 2016) and the initial learning rate is 0.2.

Table 4 reports the results for all methods, which indicate that our result outperforms all the baselines. Our method also achieves the SOTA results of 73.1% with ResNet152 as the backbone.

4.4 Experimental results on NLP dataset IMDB

Table 5: Top-1 testing accuracy(%) on imbalanced IMDB. XX denotes the CE loss or the Focal loss.

Settings	Methods	CE	Focal
Online	SGD	65.97 (± 1.12)	61.40 (± 0.58)
	ABSGD	67.13 (± 1.31)	63.80 (± 0.22)
Offline	SGD (CB-XX)	70.41 (± 0.50)	71.92 (± 0.38)
	ABSGD (CB-XX)	74.90 (± 0.56)	74.08 (± 0.76)

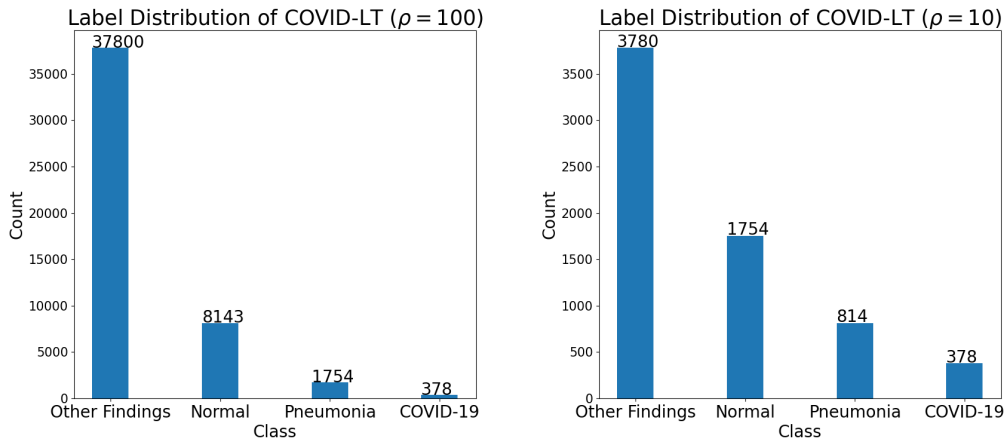


Figure 2: Label Distribution of COVID-LT with different ρ

Table 6: Top-1 testing accuracy (%) on COVID-LT with different imbalance ratio $\rho = 100$ and $\rho = 10$

Imbalance Ratio	$\rho = 100$	$\rho = 10$
SGD(CE)	54.75	58.75
ABSGD(CE)	55.75	61.75
SGD(DRW-CE)	59.25	63.75
ABSGD(CB-CE)	59.50	64.75
SGD(Focal)	54.50	58.25
ABSGD(Focal)	55.50	59.25
SGD(DRW-Focal)	60.25	62.00
ABSGD(CB-Focal)	64.00	63.50

To show the generality of ABSGD, we provide additional experiments on the sentiment analysis tasks in Natural Language Process (NLP). Internet Movie DataBase (IMDB) (Maas et al., 2011) is a large dataset of informal movie reviews with a collection of 50,000 movie reviews with 50% positive reviews and 50% negative reviews. It is equally divided into the training and testing set. To construct an imbalanced set, we remove 90% negative reviews from the training set and keep the testing set unchanged. We train the bidirectional LSTM network for 90 epochs. The initial learning rates is set 0.01, and is divided by 100, 10000 at 30th and 60th epoch, respectively. The λ is decayed at 60th epoch.

We report the top-1 testing accuracy, mean and standard deviation (std) over 5 runs, on both online and offline settings with CE and focal loss in Table 5. The improvements of ABSGD over SGD verify the effectiveness of our ABSGD method for NLP tasks.

4.5 COVID-LT: Constructed Long-Tailed COVID-19 Dataset

In this subsection, we conduct the experiments on a medical image classification task, i.e., using X-ray images to classify COVID-19. Similar tasks have been investigated in the literature (Minaee et al., 2020; Zhao et al., 2020; Cohen et al., 2020), but they mostly focus on binary classification tasks. Here, we demonstrate the effectiveness of our method for recognizing COVID-19 among other similar diseases. To this end, we construct a dataset named COVID-LT², which contains four classes of radiographs: Other Findings, Normal (No Finding), Pneumonia, COVID-19 with class index 0, 1, 2, 3. The COVID-19 images come from the

2. Label information of the dataset is available at <https://github.com/qiqi-helloworld/COVID-LT>

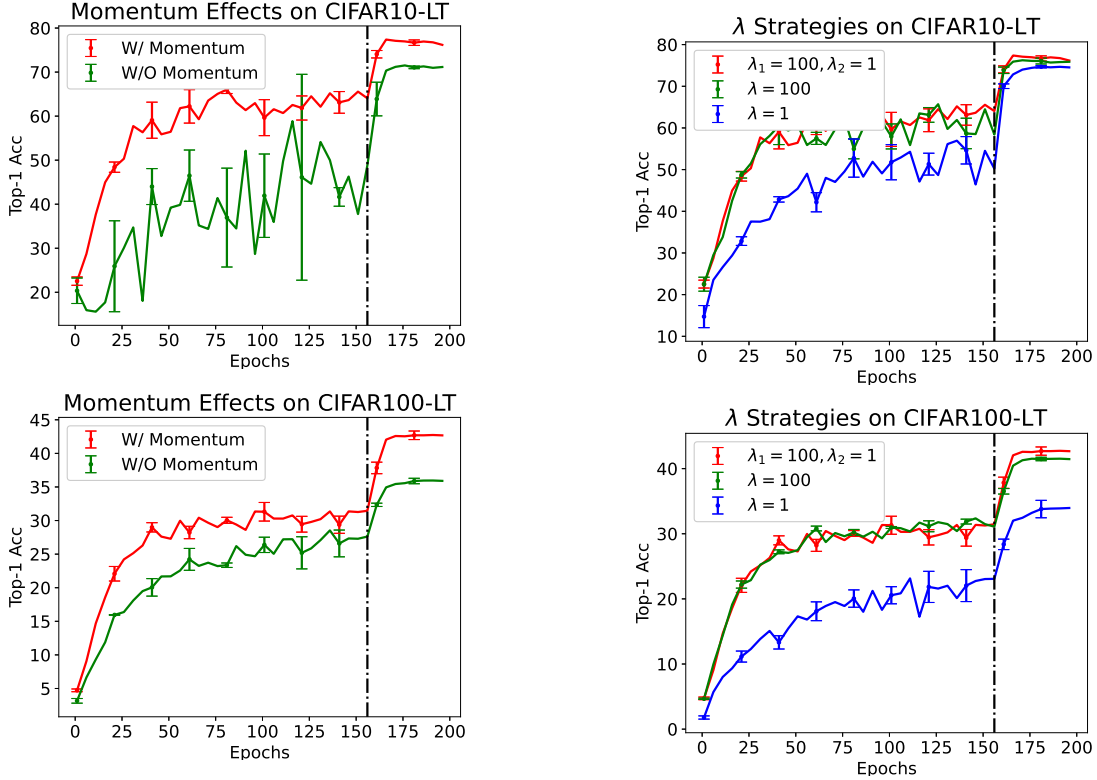


Figure 3: Ablation studies on CIFAR10-LT and CIFAR100-LT datasets: First column: comparing our method with momentum vs without momentum; Second Column: comparing our method with different strategies on setting λ . The results are averaged over 3 random trials. The black dashed lines represent the epoch where λ is decayed.

dataset collection provided by Cohen et al. (2020). The images from other three classes are extracted from the CheXpert dataset (Irvin et al., 2019). The images labeled as “other findings” include many other life-threatening diseases, e.g., Cardiomegaly, Edema. The class of (non-covid) pneumonia is included to make the task more difficult. The label distribution follows Cui et al. (2019) with the following formulation:

$$n_i = n_0 \rho^{-\frac{i}{C-1}} \quad (12)$$

where C refers to the number of classes in the dataset, $\rho = n_0/n_{C-1}$, and n_0, n_{C-1} denotes the # of samples in the most and least frequent classes, respectively. Other Findings is the most frequent class and COVID-19 is the least frequent class.

The Other Findings, Normal, Pneumonia radiographs are randomly samples from downsampled version of CheXpert (Irvin et al., 2019). There are a total of 14 observations in CheXpert, and we only keep the positive observations of Pneumonia and No Findings, while categorizing all other radiographs into Other Findings. The COVID-19 radiographs have 478 images that are collected from the positive cases of COVID-19 image data collection (Cohen et al., 2020). 378 of them are used to construct the training dataset and 100 of them are used for testing. As a result, $n_{C-1} = 378$. Then $n_0 = 37800$ when $\rho = 100$, $n_0 = 3780$ when $\rho = 10$. The label distribution of COVID-LT with different ρ is illustrated in Figure 2. Therefore COVID-LT with $\rho = 100$ contains 12875 images, and COVID-LT with $\rho = 10$ contains 4516 images. The testing set contains 100 images for each class.

We compare with baselines using momentum SGD with CE, CB-CE, Focal, CB-Focal loss for training ResNet50. In the training process, we fine tune the last block and the FC classifier layers on the ImageNet pertained ResNet50 network using SGD and ABSGD with 90 epochs. The initial learning rate is 0.1,

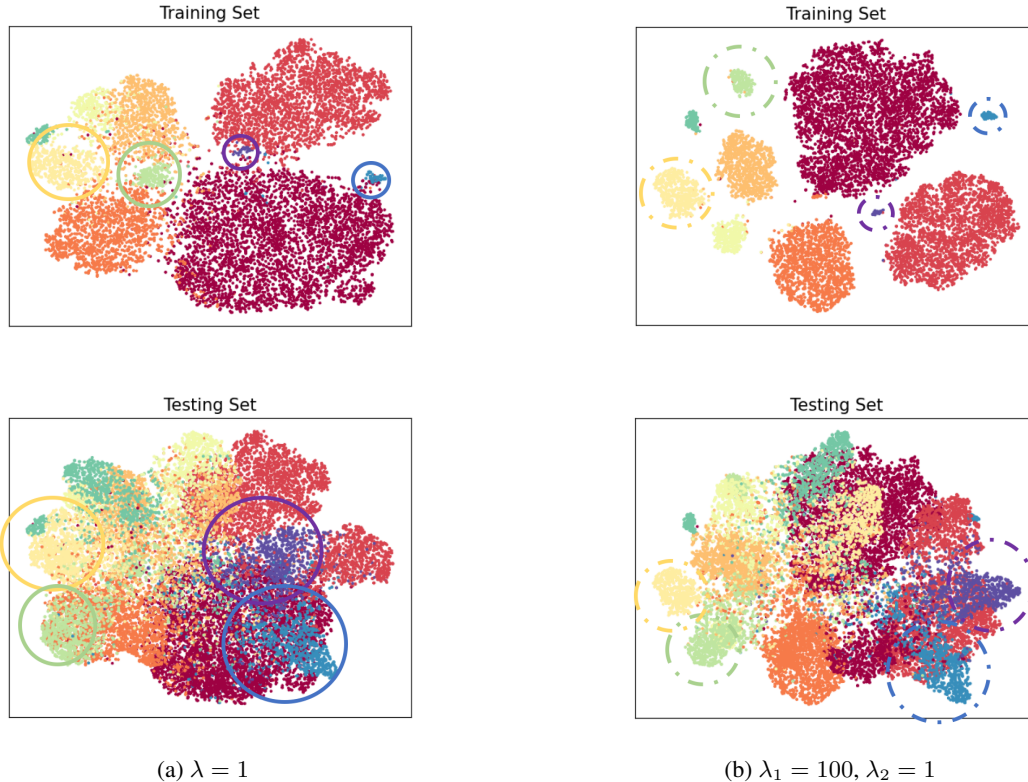


Figure 4: t-SNE visualization of training & testing set on CIFAR10-LT ($\rho = 100$) with different λ strategies.

and divide by 100, 10000 at 30th and 60th epoch, respectively. For ABSGD, λ is damped at 60th epoch. $\lambda_1 \in \{100, 200\}$, and $\lambda_2 \in \{1, 5, 10\}$. The batch size is 256. Experimental results in Table 6 verify the effectiveness of our proposed ABSGD on COVID-LT dataset.

4.6 Ablation Studies

In this section, we provide some ablation studies to verify our algorithmic choice.

The Benefit of Momentum. First, we verify that adding the momentum term can dramatically improve the performance. The results are plotted in the first column of Figure (3) on CIFAR10-LT ($\rho = 100$) and CIFAR100-LT ($\rho = 100$) datasets, where we plot the testing accuracy vs the epochs of optimization with average of 3 runs. The results clearly show that including an momentum term helps improve the performance and stabilize the training process.

The Benefit of Damping λ . Second, we verify that using the damping strategy on λ is important for improving the performance. To this end, we compare our damping strategy with that using a fixed value of λ . For the damping strategy, we use $\lambda_1 = 100$ in the first stage and $\lambda_2 = 1$ in the second stage. For fixed values of λ , we compare with $\lambda = 100$ and $\lambda = 1$. The results are plotted in the second column of Figure (3) on CIFAR10-LT and CIFAR100-LT datasets. We can see that the damping strategy is better than using a fixed value of λ , which verifies our algorithmic choice.

The Effect of Damping λ on Learned Features. Lastly, we compare the learned feature representation of using a damping strategy and a fixed value of λ . Figure 4 shows the t-SNE visualization of the learned representations of training and testing data at the end of training on the CIFAR10-LT ($\rho = 100$) with different λ strategies, where each color represents each class. Figure (4a) shows that with a fixed value $\lambda = 1$, while Figure (4b) shows that with $\lambda_1 = 100$ and $\lambda_2 = 1$ in the first and second training stage of ABSGD, respectively. It is clear to see using the damping strategy on λ yields much better feature representations that

are well separated between different classes. In contrast, the learned feature representations with a fixed value $\lambda = 1$ are more cluttered.

5. Conclusion

In this paper, we have proposed a simple momentum SGD method with self-adaptive robust weighting to tackle the data imbalance problem in deep learning. Theoretically, ABSGD is guaranteed to converge to a stationary point of a regularized distributionally robust optimization problem for learning a deep neural network. Empirically, ABSGD outperforms other weighting methods by a large margin on CIAR100-LT, Places-LT and ImageNet-LT, and matches the SOTA results when applying it with a two-stage training method on ImageNet-LT, iNaturalist18, and Places-LT.

Acknowledgement

The authors thank for the code, pretrained-models, and shared information of implementation provided by Boqing Gong from Google Research and Muhammad Abdullah Jamal from the University of Central Florida.

References

- Dzmitry Bahdanau, Kyunghyun Cho, and Yoshua Bengio. Neural machine translation by jointly learning to align and translate. *arXiv preprint arXiv:1409.0473*, 2014.
- Andrew Bud. Facing the future: The impact of apple faceid. *Biometric Technology Today*, 2018(1):5–7, 2018.
- Mateusz Buda, Atsuto Maki, and Maciej A Mazurowski. A systematic study of the class imbalance problem in convolutional neural networks. *Neural Networks*, 106:249–259, 2018.
- Róbert Busa-Fekete, Balázs Szörényi, Krzysztof Dembczynski, and Eyke Hüllermeier. Online f-measure optimization. In *Advances in Neural Information Processing Systems*, pages 595–603, 2015.
- Kaidi Cao, Colin Wei, Adrien Gaidon, Nikos Arechiga, and Tengyu Ma. Learning imbalanced datasets with label-distribution-aware margin loss. In *Advances in Neural Information Processing Systems*, pages 1567–1578, 2019.
- Robin Chan, Matthias Rottmann, Fabian Hüger, Peter Schlicht, and Hanno Gottschalk. Application of decision rules for handling class imbalance in semantic segmentation. *arXiv preprint arXiv:1901.08394*, 2019.
- Nitesh V Chawla. Data mining for imbalanced datasets: An overview. In *Data mining and knowledge discovery handbook*, pages 875–886. Springer, 2009.
- Nitesh V Chawla, Kevin W Bowyer, Lawrence O Hall, and W Philip Kegelmeyer. Smote: synthetic minority over-sampling technique. *Journal of artificial intelligence research*, 16:321–357, 2002.
- Tianyi Chen, Yuejiao Sun, and Wotao Yin. Solving stochastic compositional optimization is nearly as easy as solving stochastic optimization. *arXiv preprint arXiv:2008.10847*, 2020.
- Kyunghyun Cho, Bart Van Merriënboer, Caglar Gulcehre, Dzmitry Bahdanau, Fethi Bougares, Holger Schwenk, and Yoshua Bengio. Learning phrase representations using rnn encoder-decoder for statistical machine translation. *arXiv preprint arXiv:1406.1078*, 2014.
- Junyoung Chung, Caglar Gulcehre, KyungHyun Cho, and Yoshua Bengio. Empirical evaluation of gated recurrent neural networks on sequence modeling. *arXiv preprint arXiv:1412.3555*, 2014.

- Joseph Paul Cohen, Paul Morrison, and Lan Dao. Covid-19 image data collection. *arXiv 2003.11597*, 2020. URL <https://github.com/ieee8023/covid-chestxray-dataset>.
- Yin Cui, Menglin Jia, Tsung-Yi Lin, Yang Song, and Serge Belongie. Class-balanced loss based on effective number of samples. In *Proceedings of the IEEE Conference on Computer Vision and Pattern Recognition*, pages 9268–9277, 2019.
- Charles Elkan. The foundations of cost-sensitive learning. In *Proceedings of the 17th International Joint Conference on Artificial Intelligence - Volume 2*, pages 973–978, 2001.
- Alberto Fernández, Salvador Garcia, Francisco Herrera, and Nitesh V Chawla. Smote for learning from imbalanced data: progress and challenges, marking the 15-year anniversary. *Journal of artificial intelligence research*, 61:863–905, 2018.
- Priyal Goyal and He Kaiming. Focal loss for dense object detection. *IEEE transactions on pattern analysis and machine intelligence*, 39:2999–3007, 2018.
- Alex Graves. Generating sequences with recurrent neural networks. *arXiv preprint arXiv:1308.0850*, 2013.
- Alex Graves, Abdel-rahman Mohamed, and Geoffrey Hinton. Speech recognition with deep recurrent neural networks. In *2013 IEEE international conference on acoustics, speech and signal processing*, pages 6645–6649. IEEE, 2013.
- Hui Han, Wen-Yuan Wang, and Bing-Huan Mao. Borderline-smote: a new over-sampling method in imbalanced data sets learning. In *International conference on intelligent computing*, pages 878–887. Springer, 2005.
- Kaiming He, Xiangyu Zhang, Shaoqing Ren, and Jian Sun. Deep residual learning for image recognition. In *Proceedings of the IEEE conference on computer vision and pattern recognition*, pages 770–778, 2016.
- Chao Huang, Xian Wu, Xuchao Zhang, Suwen Lin, and Nitesh V Chawla. Deep prototypical networks for imbalanced time series classification under data scarcity. In *Proceedings of the 28th ACM International Conference on Information and Knowledge Management*, pages 2141–2144, 2019.
- Chen Huang, Yining Li, Chen Change Loy, and Xiaoou Tang. Learning deep representation for imbalanced classification. In *Proceedings of the IEEE conference on computer vision and pattern recognition*, pages 5375–5384, 2016.
- iNaturalist. The inaturalist 2018 competition dataset. 2018. URL https://github.com/visipedia/inat_comp/tree/master/2018.
- Jeremy Irvin, Pranav Rajpurkar, Michael Ko, Yifan Yu, Silvana Ciurea-Ilcus, Chris Chute, Henrik Marklund, Behzad Haghgoo, Robyn Ball, Katie Shpanskaya, et al. Chexpert: A large chest radiograph dataset with uncertainty labels and expert comparison. In *Proceedings of the AAAI Conference on Artificial Intelligence*, volume 33, pages 590–597, 2019.
- Muhammad Abdullah Jamal, Matthew Brown, Ming-Hsuan Yang, Liqiang Wang, and Boqing Gong. Rethinking class-balanced methods for long-tailed visual recognition from a domain adaptation perspective. In *Proceedings of the IEEE/CVF Conference on Computer Vision and Pattern Recognition*, pages 7610–7619, 2020.
- Justin M Johnson and Taghi M Khoshgoftaar. Survey on deep learning with class imbalance. *Journal of Big Data*, 6(1):27, 2019.
- Bingyi Kang, Saining Xie, Marcus Rohrbach, Zhicheng Yan, Albert Gordo, Jiashi Feng, and Yannis Kalantidis. Decoupling representation and classifier for long-tailed recognition. *arXiv preprint arXiv:1910.09217*, 2019.

- Salman H Khan, Munawar Hayat, Mohammed Bennamoun, Ferdous A Sohel, and Roberto Togneri. Cost-sensitive learning of deep feature representations from imbalanced data. *IEEE transactions on neural networks and learning systems*, 29(8):3573–3587, 2017.
- Yoon Kim. Convolutional neural networks for sentence classification. *arXiv preprint arXiv:1408.5882*, 2014.
- Alex Krizhevsky, Ilya Sutskever, and Geoffrey E Hinton. Imagenet classification with deep convolutional neural networks. *Communications of the ACM*, 60(6):84–90, 2017.
- Hansang Lee, Minseok Park, and Junmo Kim. Plankton classification on imbalanced large scale database via convolutional neural networks with transfer learning. In *2016 IEEE international conference on image processing (ICIP)*, pages 3713–3717. IEEE, 2016.
- Tsung-Yi Lin, Priya Goyal, Ross Girshick, Kaiming He, and Piotr Dollár. Focal loss for dense object detection. In *Proceedings of the IEEE international conference on computer vision*, pages 2980–2988, 2017.
- Charles X Ling and Victor S Sheng. Cost-sensitive learning and the class imbalance problem, 2008.
- Ziwei Liu, Zhongqi Miao, Xiaohang Zhan, Jiayun Wang, Boqing Gong, and Stella X Yu. Large-scale long-tailed recognition in an open world. In *Proceedings of the IEEE Conference on Computer Vision and Pattern Recognition*, pages 2537–2546, 2019.
- Ilya Loshchilov and Frank Hutter. Sgdr: Stochastic gradient descent with warm restarts. *arXiv preprint arXiv:1608.03983*, 2016.
- Minh-Thang Luong, Hieu Pham, and Christopher D Manning. Effective approaches to attention-based neural machine translation. *arXiv preprint arXiv:1508.04025*, 2015.
- Andrew Maas, Raymond E Daly, Peter T Pham, Dan Huang, Andrew Y Ng, and Christopher Potts. Learning word vectors for sentiment analysis. In *Proceedings of the 49th annual meeting of the association for computational linguistics: Human language technologies*, pages 142–150, 2011.
- David Masko and Paulina Hensman. The impact of imbalanced training data for convolutional neural networks, 2015.
- Shervin Minaee, Rahele Kafieh, Milan Sonka, Shakib Yazdani, and Ghazaleh Jamalipour Soufi. Deep-covid: Predicting covid-19 from chest x-ray images using deep transfer learning. *arXiv preprint arXiv:2004.09363*, 2020.
- Hongseok Namkoong and John C Duchi. Variance-based regularization with convex objectives. In *Advances in neural information processing systems*, pages 2971–2980, 2017.
- Harikrishna Narasimhan, Purushottam Kar, and Prateek Jain. Optimizing non-decomposable performance measures: A tale of two classes. In *International Conference on Machine Learning*, pages 199–208, 2015.
- Shameem Puthiya Parambath, Nicolas Usunier, and Yves Grandvalet. Optimizing f-measures by cost-sensitive classification. In *Advances in Neural Information Processing Systems (NIPS)*, pages 2123–2131, 2014.
- Omkar M Parkhi, Andrea Vedaldi, and Andrew Zisserman. Deep face recognition. 2015.
- Boris T Polyak. Some methods of speeding up the convergence of iteration methods. *USSR Computational Mathematics and Mathematical Physics*, 4(5):1–17, 1964.
- Michael I Posner, Charles R Snyder, and Brian J Davidson. Attention and the detection of signals. *Journal of experimental psychology: General*, 109(2):160, 1980.

- Qi Qi, Yan Yan, Zixuan Wu, Xiaoyu Wang, and Tianbao Yang. a simple and effective framework for pairwise deep metric learning. *arXiv preprint arXiv:1912.11194*, 2019.
- Qi Qi, Zhishuai Guo, Yi Xu, Rong Jin, and Tianbao Yang. A practical online method for distributionally deep robust optimization. *arXiv preprint arXiv:2006.10138*, 2020.
- Hassan Rafique, Mingrui Liu, Qihang Lin, and Tianbao Yang. Non-convex min-max optimization: Provable algorithms and applications in machine learning. *arXiv preprint arXiv:1810.02060*, 2018.
- Hamed Rahimian and Sanjay Mehrotra. Distributionally robust optimization: A review. *arXiv preprint arXiv:1908.05659*, 2019.
- Mirco Ravanelli, Philemon Brakel, Maurizio Omologo, and Yoshua Bengio. Light gated recurrent units for speech recognition. *IEEE Transactions on Emerging Topics in Computational Intelligence*, 2(2):92–102, 2018.
- Mengye Ren, Wenyuan Zeng, Bin Yang, and Raquel Urtasun. Learning to reweight examples for robust deep learning. *arXiv preprint arXiv:1803.09050*, 2018.
- Florian Schroff, Dmitry Kalenichenko, and James Philbin. Facenet: A unified embedding for face recognition and clustering. In *Proceedings of the IEEE conference on computer vision and pattern recognition*, pages 815–823, 2015.
- Clayton Scott. Surrogate losses and regret bounds for cost-sensitive classification with example-dependent costs. In *Proceedings of International Conference of Machine Learning (ICML)*, pages 153–160, 2011.
- Shai Shalev-Shwartz and Yonatan Wexler. Minimizing the maximal loss: How and why. In *ICML*, pages 793–801, 2016.
- Yanmin Sun, Mohamed S Kamel, Andrew KC Wong, and Yang Wang. Cost-sensitive boosting for classification of imbalanced data. *Pattern Recognition*, 40(12):3358–3378, 2007.
- Ilya Sutskever, Oriol Vinyals, and Quoc V Le. Sequence to sequence learning with neural networks. In *Advances in neural information processing systems*, pages 3104–3112, 2014.
- Yaniv Taigman, Ming Yang, Marc’Aurelio Ranzato, and Lior Wolf. Deepface: Closing the gap to human-level performance in face verification. In *Proceedings of the IEEE conference on computer vision and pattern recognition*, pages 1701–1708, 2014.
- Ashish Vaswani, Noam Shazeer, Niki Parmar, Jakob Uszkoreit, Llion Jones, Aidan N Gomez, Łukasz Kaiser, and Illia Polosukhin. Attention is all you need. *Advances in neural information processing systems*, 30: 5998–6008, 2017.
- Ashish Vaswani, Samy Bengio, Eugene Brevdo, Francois Chollet, Aidan N Gomez, Stephan Gouws, Llion Jones, Łukasz Kaiser, Nal Kalchbrenner, Niki Parmar, et al. Tensor2tensor for neural machine translation. *arXiv preprint arXiv:1803.07416*, 2018.
- Daisuke Wakabayashi. Self-driving uber car kills pedestrian in arizona, where robots roam. *The New York Times*, 19, 2018.
- Mengdi Wang, Ethan X Fang, and Han Liu. Stochastic compositional gradient descent: algorithms for minimizing compositions of expected-value functions. *Mathematical Programming*, 161(1-2):419–449, 2017.
- Yandong Wen, Kaipeng Zhang, Zhifeng Li, and Yu Qiao. A discriminative feature learning approach for deep face recognition. In *European conference on computer vision*, pages 499–515. Springer, 2016.

- Yan Yan, Tianbao Yang, Yi Yang, and Jianhui Chen. A framework of online learning with imbalanced streaming data. In *Proceedings of the Thirty-First AAAI Conference on Artificial Intelligence (AAAI)*, 2017.
- Yan Yan, Tianbao Yang, Zhe Li, Qihang Lin, and Yi Yang. A unified analysis of stochastic momentum methods for deep learning. *arXiv preprint arXiv:1808.10396*, 2018.
- Yan Yan, Yi Xu, Qihang Lin, Wei Liu, and Tianbao Yang. Sharp analysis of epoch stochastic gradient descent ascent methods for min-max optimization. *arXiv preprint arXiv:2002.05309*, 2020.
- Xi Yin, Xiang Yu, Kihyuk Sohn, Xiaoming Liu, and Manmohan Chandraker. Feature transfer learning for deep face recognition with under-represented data. *arXiv preprint arXiv:1803.09014*, 2018.
- Xiao Zhang, Zhiyuan Fang, Yandong Wen, Zhifeng Li, and Yu Qiao. Range loss for deep face recognition with long-tailed training data. In *Proceedings of the IEEE International Conference on Computer Vision*, pages 5409–5418, 2017.
- Jinyu Zhao, Yichen Zhang, Xuehai He, and Pengtao Xie. Covid-ct-dataset: a ct scan dataset about covid-19. *arXiv preprint arXiv:2003.13865*, 2020.
- Bolei Zhou, Agata Lapedriza, Aditya Khosla, Aude Oliva, and Antonio Torralba. Places: A 10 million image database for scene recognition. *IEEE transactions on pattern analysis and machine intelligence*, 40(6): 1452–1464, 2017.
- Zhi-Hua Zhou and Xu-Ying Liu. Training cost-sensitive neural networks with methods addressing the class imbalance problem. *IEEE Transactions on knowledge and data engineering*, 18(1):63–77, 2005.
- Dixian Zhu, Zhe Li, Xiaoyu Wang, Boqing Gong, and Tianbao Yang. A robust zero-sum game framework for pool-based active learning. In *The 22nd international conference on artificial intelligence and statistics*, pages 517–526, 2019.

Appendix A. Proof of Theoretical Analysis

According to the conditions of the loss function L , in Assumption 1 and Theorem 1, we first derived some properties for function $f(s) = \lambda \log(s)$ and $g(\mathbf{w}) = \exp(\frac{L(\mathbf{w}; \mathbf{z})}{\lambda})$.

Proposition 1 $g(\mathbf{w})$ is an $\frac{C^2 L}{\lambda^2}$ -smooth and $\frac{C^2 G}{\lambda^2}$ -Lipschitz continuous function.

Proof By Assumption 1 and Theorem 1, $\|\nabla L(\mathbf{w}; \mathbf{z}) - \nabla L(\mathbf{w}'; \mathbf{z})\|^2 \leq L\|\mathbf{w} - \mathbf{w}'\|^2, \forall \mathbf{w}, \mathbf{w}'$. $g(\mathbf{w}; \mathbf{z}) = \exp(\frac{L(\mathbf{w}; \mathbf{z})}{\lambda}) \leq C$, $L(\mathbf{w}; \mathbf{z}) \geq 0$ and , thus $1 \leq g(\mathbf{w}; \mathbf{z}) \leq C$. Therefore,

$$\begin{aligned} & \|\nabla g(\mathbf{w}; \mathbf{z}) - \nabla g(\mathbf{w}'; \mathbf{z})\|^2 \\ & \leq \frac{1}{\lambda^2} \|\nabla L(\mathbf{w}; \mathbf{z})^T \exp(\frac{L(\mathbf{w}; \mathbf{z})}{\lambda}) - \nabla L(\mathbf{w}'; \mathbf{z})^T \exp(\frac{L(\mathbf{w}'; \mathbf{z})}{\lambda})\|^2 \\ & \leq \frac{C^2}{\lambda^2} \|\nabla L(\mathbf{w}; \mathbf{z}) - \nabla L(\mathbf{w}'; \mathbf{z})\|^2 \leq \frac{C^2}{\lambda^2} L\|\mathbf{w} - \mathbf{w}'\|^2 \end{aligned} \quad (13)$$

In addition, with $\mathbb{E}[\|\nabla L(\mathbf{w}; \mathbf{z})\|^2] \leq G$ in Theorem 1,

$$\begin{aligned} \mathbb{E}[\|\nabla g(\mathbf{w}; \mathbf{z})\|^2] &= \frac{1}{\lambda^2} \mathbb{E}[\|\nabla L(\mathbf{w}; \mathbf{z})^T \exp(\frac{L(\mathbf{w}; \mathbf{z})}{\lambda})\|^2] \\ &\leq \frac{C^2}{\lambda^2} \mathbb{E}[\|\nabla L(\mathbf{w}; \mathbf{z})\|^2] \leq \frac{C^2 G}{\lambda^2} \leq 2C_f V_g + 2C_g L_f \mathbb{E}[\|\mathbf{y}_{t+1} - g(\mathbf{w}_t)\|^2] \end{aligned} \quad (14)$$

Proposition 2 $f(s) = \lambda \log(s)$ is an λ -smooth and λ -Lipschitz continuous function.

Proof $\nabla f(s) = \frac{\lambda}{s}$. As $s = g(\mathbf{w}; \mathbf{z}) \in (1, C]$, $\nabla f(s) \leq \lambda$, which implies $\|\nabla f(s)\| \leq \lambda$. In addition,

$$\|\nabla f(s_1) - \nabla f(s_2)\| = \left\| \frac{\lambda}{s_1} - \frac{\lambda}{s_2} \right\| \leq \left\| \frac{\lambda}{s_1 s_2} \right\| \|s_1 - s_2\| \leq \lambda \|s_1 - s_2\|. \quad (15)$$

In the following proof, we denote, $L_g = C^2 L, C_g = C^2 G, C_f = \lambda, L_f = \lambda$. Further denote $\bar{L} = C_g L_f + C_f L_g$

Lemma 1 Let \mathbf{p}_t be

$$\mathbf{p}_t = \begin{cases} \frac{\beta}{1-\beta}(\mathbf{w}_t - \mathbf{w}_{t-1}) & t \geq 1 \\ 0 & t = 0 \end{cases} \quad (16)$$

$\mathbf{q}_t = \mathbf{w}_t + \mathbf{p}_t$, and $\mathbf{v}_t = \frac{1-\beta}{\beta} \mathbf{p}_t$. Then

$$\mathbf{q}_{t+1} = \mathbf{q}_t - \frac{\eta}{1-\beta} \mathcal{G}(\mathbf{w}_t) \quad (17)$$

$$\mathbf{v}_{t+1} = \beta \mathbf{v}_t - \eta \mathcal{G}(\mathbf{w}_t) \quad (18)$$

where $\mathcal{G}(\mathbf{w}_t) = \nabla g_\xi(\mathbf{w}_t) \nabla f(\mathbf{y}_{t+1})$, ξ represents a random sample from $\{\mathbf{z}_1, \dots, \mathbf{z}_n\}$.

Remark: The proof is the same as Lemma1 of Yan et al. (2018), we omitted the proof here.

Before we move on, we derive some inequalities that are helpful for later proofs. By ABSGD(Algorithm 1), $\nabla F(\mathbf{q}_t) = \nabla f(g(\mathbf{q}_t))^T \nabla g(\mathbf{q}_t)$ for $\mathbf{q}_t = \mathbf{w}_t + \mathbf{p}_t$. Then for any iteration $t = 1 \dots T$ in ABSGD, the following inequality holds for $\delta_t = \nabla f(\mathbf{y}_{t+1})^T \nabla g_\xi(\mathbf{w}_t) - \nabla f(g(\mathbf{w}_t))^T \nabla g(\mathbf{w}_t)$

$$\begin{aligned} \|\mathbb{E}[\delta_t]\| &= \|\nabla g(\mathbf{w}_t)^T \mathbb{E}[\nabla f(\mathbf{y}_{t+1})] - \nabla f(g(\mathbf{w}_t))^T \nabla g(\mathbf{w}_t)\| \\ &\leq \|\nabla g(\mathbf{w}_t)\| \mathbb{E}[\|\nabla f(\mathbf{y}_{t+1}) - \nabla f(g(\mathbf{w}_t))\|] \leq \|\nabla g(\mathbf{w}_t)\| \sqrt{L_f} \mathbb{E}[\|\mathbf{y}_{t+1} - g(\mathbf{w}_t)\|] \end{aligned} \quad (19)$$

$$\begin{aligned}
\mathbb{E}[\|\delta_t\|^2] &= \mathbb{E}[\|\nabla f(\mathbf{y}_{t+1})^T g_\xi(\mathbf{w}_t) - \nabla f(g(\mathbf{w}_t))^T \nabla g(\mathbf{w}_t)\|^2] \\
&\leq 2\mathbb{E}[\|\nabla f(\mathbf{y}_{t+1})^T g_\xi(\mathbf{w}_t) - \nabla f(\mathbf{y}_{t+1})^T \nabla g(\mathbf{w}_t)\|^2] \\
&\quad + 2\mathbb{E}[\|\nabla g(\mathbf{w}_t)^T \nabla f(\mathbf{y}_{t+1}) - \nabla f(g(\mathbf{w}_t))^T \nabla g(\mathbf{w}_t)\|^2] \\
&\leq 2C_f V_g + 2C_g L_f \mathbb{E}[\|\mathbf{y}_{t+1} - g(\mathbf{w}_t)\|^2]
\end{aligned} \tag{20}$$

$$\begin{aligned}
\mathbb{E}[\|\mathcal{G}(\mathbf{w}_t)\|^2] &\leq 2\mathbb{E}[\|\mathcal{G}(\mathbf{w}_t) - \nabla g(\mathbf{w}_t)^T \nabla f(g(\mathbf{w}_t))\|^2] + 2\mathbb{E}[\|\nabla g(\mathbf{w}_t)^T \nabla f(g(\mathbf{w}_t))\|^2] \\
&\leq 4\mathbb{E}[\|\mathcal{G}(\mathbf{w}_t) - \nabla g(\mathbf{w}_t)^T \nabla f(\mathbf{y}_{t+1})\|^2] + 4\mathbb{E}[\|\nabla g(\mathbf{w}_t)^T \nabla f(\mathbf{y}_{t+1}) - \nabla g(\mathbf{w}_t)^T \nabla f(g(\mathbf{w}_t))\|^2] \\
&\quad + 2\mathbb{E}[\|\nabla g(\mathbf{w}_t)^T \nabla f(g(\mathbf{w}_t))\|^2] \leq 4C_g L_f \|\mathbf{y}_{t+1} - g(\mathbf{w}_t)\|^2 + 4C_f V_g + 2C_f C_g
\end{aligned} \tag{21}$$

By Lemma 4 in (Yan et al., 2018), we have

$$\begin{aligned}
\|\nabla F(\mathbf{q}_t) - \nabla F(\mathbf{w}_t)\|^2 &= \|\nabla g(\mathbf{q}_t) \nabla f(g(\mathbf{q}_t)) - \nabla g(\mathbf{w}_t) \nabla f(g(\mathbf{w}_t))\|^2 \\
&= \|\nabla g(\mathbf{q}_t) \nabla f(g(\mathbf{q}_t)) - \nabla g(\mathbf{q}_t) \nabla f(g(\mathbf{w}_t)) + \nabla g(\mathbf{q}_t) \nabla f(g(\mathbf{w}_t)) - \nabla g(\mathbf{w}_t) \nabla f(g(\mathbf{w}_t))\|^2 \\
&\leq C_g L_f \|\mathbf{q}_t - \mathbf{w}_t\|^2 + C_f L_g \|\mathbf{q}_t - \mathbf{w}_t\|^2 \leq \bar{L} \|\mathbf{q}_t - \mathbf{w}_t\|^2
\end{aligned} \tag{22}$$

$$\|\nabla F(\mathbf{q}_t) - \nabla F(\mathbf{w}_t)\|^2 \leq \bar{L} \|\mathbf{q}_t - \mathbf{w}_t\|^2 \leq \frac{\bar{L}^2 \beta^2}{(1-\beta)^2} \mathbb{E}[\|\mathbf{v}_t\|^2] \leq \frac{\bar{L}^2 \beta^2}{(1-\beta)^2} \frac{1-\beta^t}{1-\beta} \sum_{\tau=1}^t \beta^{t-\tau} \eta^2 \|\mathcal{G}(\mathbf{w}_\tau)\|^2 \tag{23}$$

$$\begin{aligned}
\gamma^{-1} \|\mathbf{w}_{t+1} - \mathbf{w}_t\|^2 &= \gamma^{-1} \left\| \sum_{\tau=0}^t \beta^{t-\tau} \eta \mathcal{G}(\mathbf{w}_\tau) \right\|^2 = \gamma^{-1} \frac{(1-\beta^t)^2}{(1-\beta)^2} \left\| \frac{1-\beta}{1-\beta^t} \sum_{\tau=0}^t \beta^{t-\tau} \eta \mathcal{G}(\mathbf{w}_\tau) \right\|^2 \\
&\leq \gamma^{-1} \frac{(1-\beta^t)}{(1-\beta)} \sum_{\tau=0}^t \beta^{t-\tau} \|\eta \mathcal{G}(\mathbf{w}_\tau)\|^2 \leq \frac{\gamma^{-1} \eta^2}{(1-\beta)} \sum_{\tau=0}^t \beta^{t-\tau} \|\mathcal{G}(\mathbf{w}_\tau)\|^2
\end{aligned} \tag{24}$$

where the first inequality applies the convexity of $\|\cdot\|$.

Then take the summation over all iterations, $1 \cdots T$, we have

$$\begin{aligned}
\sum_{t=1}^T \gamma^{-1} \|\mathbf{w}_{t+1} - \mathbf{w}_t\|^2 &\leq \frac{\eta^2}{1-\beta} \sum_{t=1}^T \left(\sum_{\tau=t}^T \gamma^{-1} \beta^{\tau-t} \right) \|\mathcal{G}(\mathbf{w}_t)\|^2 \\
&\leq \frac{\eta^2}{1-\beta} \sum_{k=1}^T \gamma^{-1} (4C_g L_f \|\mathbf{y}_{t+1} - g(\mathbf{w}_t)\|^2 + 4C_f V_g + 2C_f C_g) \\
&\leq \frac{\eta^2}{1-\beta} \sum_{k=1}^T \gamma^{-1} (4C_g L_f D_{\mathbf{y}} + 4C_f V_g + 2C_f C_g)
\end{aligned} \tag{25}$$

Lemma 2 Let $\mathbf{q}_t = \mathbf{w}_t + \mathbf{p}_t$, $\delta_t = \mathcal{G}(\mathbf{w}_t) - \nabla g(\mathbf{w}_t)^T \nabla f(g(\mathbf{w}_t))$ for any $t \in 1, \dots, T$

$$\begin{aligned}
\mathbb{E}[f(\mathbf{q}_{t+1}) - f(\mathbf{q}_t)] &\leq \left(\frac{\eta^2 L}{(1-\beta)^2} - \frac{\eta}{1-\beta} + \frac{\eta^2}{(1-\beta)^2} \frac{1}{\gamma} \right) \mathbb{E}[\|\nabla F(\mathbf{w}_t)\|^2] \\
&\quad + \frac{1}{L} \|\nabla F(\mathbf{q}_t) - \nabla F(\mathbf{w}_t)\|^2 + \left(\gamma + \frac{\eta^2 L}{2(1-\beta)^2} \right) C_g L_f \mathbb{E}[\|\mathbf{y}_{t+1} - g(\mathbf{w}_t)\|^2]
\end{aligned} \tag{26}$$

Proof:

$$\begin{aligned}
f(\mathbf{q}_{t+1}) &\leq f(\mathbf{q}_t) + \langle \nabla F(\mathbf{q}_t), \mathbf{q}_{t+1} - \mathbf{q}_t \rangle + \frac{L\|\mathbf{q}_{t+1} - \mathbf{q}_t\|^2}{2} \\
&= f(\mathbf{q}_t) - \frac{\eta}{1-\beta} \nabla F(\mathbf{q}_t)^T \mathcal{G}(\mathbf{w}_t) + \frac{L\eta^2 \|\mathcal{G}(\mathbf{w}_t)\|^2}{2(1-\beta)^2} \\
&= f(\mathbf{q}_t) - \frac{\eta}{1-\beta} \nabla F(\mathbf{q}_t)^T \delta_t - \frac{\eta}{1-\beta} \nabla F(\mathbf{q}_t)^T \nabla F(\mathbf{w}_t) + \frac{L\eta^2 \|\mathcal{G}(\mathbf{w}_t) - \nabla F(\mathbf{w}_t) + \nabla F(\mathbf{w}_t)\|^2}{2(1-\beta)^2} \\
&\leq \mathbb{E}[-\frac{\alpha}{1-\beta} \nabla F(\mathbf{q}_t)^T \delta_t - \frac{\alpha}{1-\beta} (\nabla F(\mathbf{q}_t) - \nabla F(\mathbf{w}_t))^T \nabla F(\mathbf{w}_t) \\
&\quad - (\frac{\alpha}{1-\beta} - \frac{L}{2} \frac{\alpha^2}{(1-\beta)^2}) \|\nabla F(\mathbf{w}_t)\|^2] + \frac{L}{1} \frac{\alpha^2}{(1-\beta)^2} \mathbb{E}[\|\delta_t\|^2] \\
&\stackrel{(20)}{\leq} \underbrace{\mathbb{E}[-\frac{\alpha}{1-\beta} \nabla F(\mathbf{q}_t)^T \delta_t + \frac{1}{2L} \|\nabla F(\mathbf{q}_t) - \nabla F(\mathbf{w}_t)\|^2]}_{\textcircled{1}} - (\frac{\alpha}{1-\beta} - \frac{\alpha^2 L}{(1-\beta)^2}) \|\nabla F(\mathbf{w}_t)\|^2 \\
&\quad + \frac{\alpha^2 L}{(1-\beta)^2} (2C_f V_g + 2C_g L_f \mathbb{E}[\|\mathbf{y}_{t+1} - g(\mathbf{w}_t)\|^2])
\end{aligned} \tag{27}$$

Where the first inequality applies the smoothness property of the objective f . The first equality is due to Lemma 1. Then for the first cross term $\textcircled{1}$ on the right hand side above equation, we have

$$\begin{aligned}
\textcircled{1} &= \mathbb{E}[-\frac{\eta}{1-\beta} \nabla F(\mathbf{q}_t)^T \delta_t] = \mathbb{E}[-\frac{\eta}{1-\beta} (\nabla F(\mathbf{q}_t) - \nabla F(\mathbf{w}_t) + \nabla F(\mathbf{w}_t))^T \delta_t] \\
&= \mathbb{E}[-\frac{\eta}{1-\beta} (\nabla F(\mathbf{q}_t) - \nabla F(\mathbf{w}_t))^T \delta_t] - \mathbb{E}[\frac{\eta}{1-\beta} \nabla F(\mathbf{w}_t)^T \delta_t] \\
&\leq \mathbb{E}[-\frac{\eta}{1-\beta} (\nabla F(\mathbf{q}_t) - \nabla F(\mathbf{w}_t))^T \delta_t] + \frac{\eta}{1-\beta} \|\nabla F(\mathbf{w}_t)\| \sqrt{C_g L_f} \mathbb{E}[\|\mathbf{y}_{t+1} - g(\mathbf{w}_t)\|] \\
&\leq \mathbb{E}[-\frac{\eta}{1-\beta} (\nabla F(\mathbf{q}_t) - \nabla F(\mathbf{w}_t))^T \delta_t] + \frac{\eta^2}{(1-\beta)^2} \frac{1}{\gamma} \|\nabla F(\mathbf{w}_t)\|^2 + \gamma C_g L_f \mathbb{E}[\|\mathbf{y}_{t+1} - g(\mathbf{w}_t)\|^2] \\
&\leq \frac{1}{2L} \|\nabla F(\mathbf{q}_t) - \nabla F(\mathbf{w}_t)\|^2 + \frac{\eta^2}{(1-\beta)^2} \frac{1}{\gamma} \|\nabla F(\mathbf{w}_t)\|^2 + (\gamma + \frac{\eta^2 L}{2(1-\beta)^2}) C_g L_f \mathbb{E}[\|\mathbf{y}_{t+1} - g(\mathbf{w}_t)\|^2]
\end{aligned} \tag{28}$$

Plugging it back, we have

$$\begin{aligned}
\mathbb{E}[f(\mathbf{q}_{t+1}) - f(\mathbf{q}_t)] &\leq (\frac{\alpha^2 L}{(1-\beta)^2} - \frac{\alpha}{1-\beta} + \frac{\eta^2}{(1-\beta)^2} \frac{1}{\gamma}) \mathbb{E}[\|\nabla F(\mathbf{w}_t)\|^2] \\
&\quad + \frac{1}{L} \|\nabla F(\mathbf{q}_t) - \nabla F(\mathbf{w}_t)\|^2 + (\gamma + \frac{\eta^2 L}{2(1-\beta)^2}) C_g L_f \mathbb{E}[\|\mathbf{y}_{t+1} - g(\mathbf{w}_t)\|^2]
\end{aligned} \tag{29}$$

Combining equation (29) and (22), we finish the proof of the lemma.

$$\mathbb{E}[\|\nabla f(\mathbf{q}_t) - \nabla f(\mathbf{w}_t)\|^2] \leq L^2 \|\mathbf{p}_t\|^2 = \frac{L^2 \beta^2}{(1-\beta)^2} \mathbb{E}[\|\mathbf{v}_t\|^2] \tag{30}$$

Lemma 3 By running algorithm 1, for $\forall, 1 \dots T$,

$$\begin{aligned}
\mathbb{E}[\|\mathbf{y}_{t+1} - g(\mathbf{w}_t)\|^2] &\leq (1-\gamma) \|\mathbf{y}_t - g(\mathbf{w}_{t-1})\|^2 \\
&\quad + \gamma^{-1} C_g \|\mathbf{w}_t - \mathbf{w}_{t-1}\|^2 + 2V_g \gamma^2
\end{aligned} \tag{31}$$

In addition, $\mathbb{E}[\|\mathbf{y}_{t+1} - g(\mathbf{w}_t)\|^2] \leq D_y \forall, t \in \{1, \dots, T\}$, where $D_y = 1 + 4C_g L_f \mathbb{E}[\|\mathbf{y}_1 - g(\mathbf{w}_0)\|^2] + C_g(2V_g + C_f V_g + 2C_f)$. And $\mathbb{E}[\|\mathcal{G}(\mathbf{w}_t)\|^2] \leq C_f V_g + 4C_g L_f \|\mathbf{y}_{t+1} - g(\mathbf{w}_t)\|^2 + 2C_g C_f \leq D_y$

Proof:

Denote $e_t = (1 - \gamma)(g(\mathbf{w}_t) - g(\mathbf{w}_{t-1}))$. By Updates of ABSGD (Algorithm 1)

$$\mathbf{y}_{t+1} = (1 - \gamma)\mathbf{y}_t + \gamma g_\xi(\mathbf{w}_t) \quad (32)$$

$$\mathbf{y}_{t+1} - g(\mathbf{w}_t) + e_t \stackrel{(32)}{=} (1 - \gamma)(\mathbf{y}_t - g(\mathbf{w}_{t-1})) + \gamma(g_\xi(\mathbf{w}_t) - g(\mathbf{w}_t)) \quad (33)$$

Therefore,

$$\begin{aligned} \mathbb{E}[\|\mathbf{y}_{t+1} - g(\mathbf{w}_t) + e_t\|^2] &= \mathbb{E}[(1 - \gamma)^2 \|\mathbf{y}_t - g(\mathbf{w}_{t-1})\|^2 + \gamma^2 \|g_\xi(\mathbf{w}_t) - g(\mathbf{w}_t)\|^2] \\ &\leq (1 - \gamma)^2 \|\mathbf{y}_t - g(\mathbf{w}_{t-1})\|^2 + \gamma^2 V_g \end{aligned} \quad (34)$$

where the first equality holds due to $\mathbb{E}[\langle \mathbf{y}_t - g(\mathbf{w}_{t-1}), g_\xi(\mathbf{w}_t) - g(\mathbf{w}_t) \rangle] = 0$. In addition, by $\|a + b\|^2 \leq (1 + \epsilon)\|a\|^2 + (1 + 1/\epsilon)\|b\|^2$, we have

$$\mathbb{E}[\|\mathbf{y}_{t+1} - g(\mathbf{w}_t)\|^2] \leq (1 + \gamma)\mathbb{E}[\|\mathbf{y}_{t+1} - g(\mathbf{w}_t) + e_t\|^2] + (1 + 1/\gamma)\mathbb{E}[\|e_t\|^2] \quad (35)$$

Combining equation (34) and (35):

$$\mathbb{E}[\|\mathbf{y}_{t+1} - g(\mathbf{w}_t)\|^2] \leq \mathbb{E}[(1 - \gamma)\|\mathbf{y}_t - g(\mathbf{w}_{t-1})\|^2] + 2\gamma^2 V_g + \gamma^{-1} C_g \|\mathbf{w}_t - \mathbf{w}_{t-1}\|^2 \quad (36)$$

$$D_y = \underbrace{(1 + 4C_g L_f) \mathbb{E}[\|\mathbf{y}_1 - g(\mathbf{w}_0)\|^2]}_A + 2C_f C_g + 2C_f V_g + 2V_g \quad (37)$$

$$\mathbb{E}[\|\mathcal{G}(\mathbf{w}_t)\|^2] \leq 4C_g L_f \|\mathbf{y}_{t+1} - g(\mathbf{w}_t)\|^2 + 2C_g C_f + C_f V_g \quad (38)$$

We show by induction that $\mathbb{E}[\|\mathbf{y}_{t+1} - g(\mathbf{w}_t)\|^2] \leq D_y$ for all $t = 1, \dots, T$.

Suppose that $\|\mathbf{y}_t - g(\mathbf{w}_{t-1})\|^2 \leq D_y$, then

$$\begin{aligned} \mathbb{E}[\|\mathbf{y}_{t+1} - g(\mathbf{w}_t)\|^2] &\leq \mathbb{E}[(1 - \gamma)D_y + \frac{\alpha_t^2}{\gamma}(4C_g L_f D_y + 2C_f V_g + 2C_g C_f)] + 2\gamma^2 V_g \\ &\leq D_y - \gamma D_y + \underbrace{\frac{\alpha_t^2}{\gamma}(4C_g L_f D_y + 2C_f V_g + 2C_g C_f)}_B + 2\gamma^2 V_g \end{aligned} \quad (39)$$

With $\eta = \frac{1}{T^{3/4}}, \gamma = \frac{1}{T^{1/2}}, \frac{\eta^2}{\gamma} = \frac{1}{T}$. Assume that $4C_g C_f \leq T^{1/2}/2$, and $T \geq 16$, we have $\frac{\eta^2}{\gamma} 4C_g L_f \leq \gamma, \frac{\eta^2}{\gamma}(1 + 4C_f C_g) \leq \gamma, \frac{\eta^2}{\gamma} 4C_g L_f + \gamma^2 \leq \gamma$. Then

$$B = -(\gamma - \frac{\eta^2}{\gamma} 4C_g L_f)A - (\gamma - \frac{\eta^2}{\gamma} - 4C_g L_f \frac{\eta^2}{\gamma})(2C_f C_g + 2C_f V_g) - (\gamma - 4C_g L_f \frac{\eta^2}{\gamma} - \gamma^2)2V_g \leq 0 \quad (40)$$

As a result, $\mathbb{E}[\|\mathbf{y}_{t+1} - g(\mathbf{w}_t)\|^2] \leq D_y$.

A.1 Proof of Theorem 1

Proof: Suppose that 1) $\frac{L\eta^2}{2(1-\beta)^2} + \frac{\eta^2}{(1-\beta\eta)^2} \frac{1}{\gamma} \leq \frac{1}{2} \frac{\eta}{1-\beta}$. 2) $\mathbb{E}[\|\mathbf{y}_{t+1} - g(\mathbf{w}_t)\|^2] \leq D_y$, for $\forall t \in \{1, \dots, T\}$, $J_t = f(\mathbf{q}_t) + \|\mathbf{y}_t - g(\mathbf{w}_{t-1})\|^2$. By Lemma 2 and Lemma 3, multiply $(1 + \gamma_t)$ for equation (31) and adding together with equation (26):

$$\begin{aligned} f(\mathbf{q}_{t+1}) + (1 + \gamma)\|\mathbf{y}_{t+1} - g(\mathbf{w}_t)\|^2 &\leq f(\mathbf{q}_t) + (1 - \gamma^2)\|\mathbf{y}_t - g(\mathbf{w}_{t-1})\|^2 + (1 + \gamma)\gamma^{-1} C_g \|\mathbf{w}_t - \mathbf{w}_{t-1}\|^2 \\ &+ (1 + \gamma)2V_g \gamma^2 - \frac{2\eta}{1-\beta} \mathbb{E}[\|\nabla F(\mathbf{w}_t)\|^2] + \frac{L\eta^2}{(1-\beta)^2} \sigma^2 + L\|\mathbf{q}_t - \mathbf{w}_t\|^2 + (\gamma + \frac{\eta^2 L}{2(1-\beta)^2}) C_g^2 L_f^2 \mathbb{E}[\|\mathbf{y}_{t+1} - g(\mathbf{w}_t)\|^2] \end{aligned} \quad (41)$$

$$\begin{aligned}
J_{t+1} &\leq J_t + 2\gamma^{-1}C_g\|\mathbf{w}_t - \mathbf{w}_{t-1}\|^2 + 4V_g\gamma^2 - 2\frac{\alpha_t}{(1-\beta)}\mathbb{E}[\|\nabla F(\mathbf{w}_t)\|^2] \\
&\quad + \frac{L\eta^2}{(1-\beta)^2}(\sigma^2 + D_{\mathbf{y}}) + L\|\mathbf{z}_t - \mathbf{w}_t\|^2
\end{aligned} \tag{42}$$

Rearranging terms and summation from $1, \dots, T$,

$$\begin{aligned}
\sum_{t=1}^T \mathbb{E}[\eta\|\nabla F(\mathbf{w}_t)\|^2] &\leq \frac{(1-\beta)}{2} \sum_{t=1}^T (J_t - J_{t+1}) + (1-\beta)C_g \sum_{t=1}^T \gamma^{-1}\|\mathbf{w}_t - \mathbf{w}_{t-1}\|^2 \\
&\quad + L \sum_{t=1}^T \|\mathbf{q}_t - \mathbf{w}_t\|^2 + 4V_g \sum_{t=1}^T \gamma^2 + \frac{T\eta^2 L}{(1-\beta)^2}(\sigma^2 + D_{\mathbf{y}})
\end{aligned} \tag{43}$$

Next we bound the terms in the right hand size of the equation (43). Taking the summation of equation (24) from $1, \dots, T$,

$$\begin{aligned}
\sum_{t=1}^T \gamma^{-1}\|\mathbb{E}[\mathbf{w}_{t+1} - \mathbf{w}_t]\|^2 &= \sum_{t=1}^T \frac{\gamma^{-1}}{1-\beta} \sum_{\tau=0}^t \beta^{t-\tau} \eta^2 \mathbb{E}[\|\mathcal{G}(\mathbf{w}_\tau)\|^2] \leq \frac{\gamma}{1-\beta} \sum_{t=1}^T \eta^2 \left(\sum_{\tau=t}^T \beta^{\tau-t} \right) \mathbb{E}[\|\mathcal{G}(\mathbf{w}_t)\|^2] \\
&\leq \frac{\gamma}{(1-\beta)^2} \sum_{t=1}^T \eta^2 \mathbb{E}[\|\mathcal{G}(\mathbf{w}_t)\|^2] \leq \frac{\gamma}{(1-\beta)^2} \sum_{t=1}^T \eta^2 D_{\mathbf{y}}
\end{aligned} \tag{44}$$

where the last inequality is due to Lemma 3.

Taking the summation of equation (23) from $1, \dots, T$,

$$\begin{aligned}
\sum_{k=1}^T L^2 \|\mathbf{q}_t - \mathbf{w}_t\|^2 &\leq \frac{L^2 \beta^2}{(1-\beta)^3} \sum_{t=1}^T \sum_{\tau=1}^t \beta^{t-\tau} \eta^2 \|\mathcal{G}(\mathbf{w}_\tau)\|^2 = \frac{L^2 \beta^2}{(1-\beta)^3} \sum_{t=1}^T \left(\sum_{\tau=t}^T \beta^{T-\tau} \right) \eta^2 \|\mathcal{G}(\mathbf{w}_\tau)\|^2 \\
&\leq \frac{L^2 \beta^2}{(1-\beta)^4} \sum_{t=1}^T \eta^2 \|\mathcal{G}(\mathbf{w}_t)\|^2 \leq \frac{L^2 \beta^2}{(1-\beta)^4} \eta^2 T D_{\mathbf{y}}
\end{aligned} \tag{45}$$

Plugging above equations (45) and (44) to equation (43),

$$\begin{aligned}
\sum_{t=1}^T \mathbb{E}[\eta\|\nabla f(\mathbf{w}_t)\|^2] &\leq \frac{(1-\beta)}{2} J_0 + \frac{C_g \gamma^{-1}}{1-\beta} \eta^2 T + \frac{L^2 \beta^2}{(1-\beta)^4} \eta^2 T D_{\mathbf{y}} + 4V_g \sum_{t=1}^T \gamma^2 + \frac{L}{(1-\beta)^2} (V_g^2 + D_{\mathbf{y}}) \eta^2 T \\
\frac{1}{T^{3/4}} \sum_{t=1}^T \mathbb{E}[\|\nabla f(\mathbf{w}_t)\|^2] &\leq \frac{(1-\beta)}{2} J_0 + \frac{C_g}{1-\beta} + 4V_g + \frac{L^2 \beta^2 D_{\mathbf{y}}}{(1-\beta)^4} \frac{1}{T^{1/2}} + \frac{L}{(1-\beta)^2} (V_g^2 + D_{\mathbf{y}}) \frac{1}{T^{1/2}}
\end{aligned} \tag{46}$$

Then multiply $\frac{1}{T^{1/4}}$ on both side and exhibit all the constant factor with big O , we have the result.

Appendix B. Two-Stage Experimental Results on Places-LT and ImageNet-LT

Following similar setting as section 4.3, we compare ABSGD with SOTA methods at this section by combine the two-stage training trick proposed in Kang et al. (2019).i.e, we train the (last block of) feature representation in the first stage and fine-tune the classifier in the second and third stages of ABSGD. In particular, we train the last block of the convolutions layer and fully connected layer for 90 epochs in the first stage with $\lambda_1 = 1000$ from the pretrained model on ImageNet for Places-LT, and retrain the fully connected layer for 20 and 10 epochs in second and third stage of ABSGD with $\lambda_2 \in \{100, 200\}$ and $\lambda_3 \in \{1, 5, 10\}$, respectively. For ImageNet-LT, we jointly train the feature representation and classifier in the first stage for 90 epochs from

scratch, and retrain the fully connected layer for 60 and 30 epochs of ABSGD in the second and third stages with $\lambda_2 = \{100, 200\}$ and $\lambda_3 = \{1, 5, 10\}$, respectively. The initial learning rate is 0.2 for ImageNet-LT and 0.01 for Places-LT. We apply the cosine annealing schedule (Loshchilov and Hutter, 2016) in the training process, and reset the the learning rate at the start of second stages. The mini-batch size is 512. Experimental results are reported in Table 7 and Table 8.

Table 7: Test top-1 accuracy(%) of different SOTA methods on Places-LT using ResNet50 with ImageNet pretrained initialization. TV represents Trainable Variable, CB denotes Class-Balanced Sampling (Cui et al., 2019), FC represents fully connected layer, LB represents the last block in the backbone. * denotes an additional memory is required in the second stage and \dagger represents an additional balanced data set is required in the second stage.

Methods	Sampling	Loss	Stage-1 TV	Stage-2 TV	Results
Vanilla Model (Jamal et al., 2020)	CB	CE	FC/LB+FC	-	27.9/30.3
Vanilla Model (Lin et al., 2017)	CB	Focal	FC/LB+FC	-	33/33.5
Vanilla Model (Zhang et al., 2017)	CB	Range	FC		35.1
Joint (Kang et al., 2019)	CB	CE	LB+FC	LB+FC	30.2
NCM (Kang et al., 2019)	CB	CE	LB+FC	FC	36.3
cRT (Kang et al., 2019)	CB	CE	LB+FC	FC	36.7
τ -normalized (Kang et al., 2019)	CB	CE	LB+FC	FC	37.9
OLTR* (Liu et al., 2019)	CB	CE	LB+FC	FC	35.9
META \dagger (Jamal et al., 2020)	None	CE	LB+FC	FC	37.1
ABSGD	None	CE	LB+FC	FC	37.7

Table 7 reports the experimental results on Places-LT. τ -normalization method proposed in (Kang et al., 2019) has the best reported SOTA result. However, it is obvious to see that ABSGD outperforms the META methods by a relatively large margin of 0.6% with standard CE loss on Places-LT after applying the two-stage training trick on both methods. The results is consistency with the results in Table 3, which verifies that ABSGD is more effective than META methods on Places-LT with CE loss. In Table 8, ABSGD has the same results as the SOTA results achieved by the META method on ImageNet-LT and has no requirements on the additional balanced validation datasets.

Table 8: Test top-1 accuracy(%) of different SOTA methods on ImageNet-LT with Resnet50 training from scratch. TV represents Trainable Variable, CB denotes Class-Balanced Sampling (Cui et al., 2019), FC represents fully connected layer, LB represents the last block in the backbone. \dagger represents an additional balanced data set is required in the second stage.

Methods	Sampling	Loss	Stage-1 TV	Stage-1 TV	Results
Vanilla Model (Jamal et al., 2020)	None	CE	All	-	41.0
CB (Cui et al., 2019)	None	CE	All	-	41.8
Joint (Kang et al., 2019)	CB	CE	All	All	41.6
NCM (Kang et al., 2019)	CB	CE	All	FC	44.3
cRT (Kang et al., 2019)	CB	CE	All	FC	43.3
τ -normalizer (Kang et al., 2019)	CB	CE	All	FC	46.7
META \dagger (Jamal et al., 2020)	None	CE	All	FC	48.0
ABSGD	None	CE	All	FC+LB	48.0